



Seven ferroptosis-specific expressed genes are considered as potential biomarkers for the diagnosis and treatment of cigarette smoke-induced chronic obstructive pulmonary disease

Zhiwei Lin[#], Yifan Xu[#], Lili Guan[#], Lijie Qin, Jiabin Ding, Qingling Zhang, Luqian Zhou

State Key Laboratory of Respiratory Disease, National Clinical Research Center for Respiratory Disease, Guangzhou Institute of Respiratory Health, First Affiliated Hospital of Guangzhou Medical University, Guangzhou, China

Contributions: (I) Conception and design: L Zhou, Q Zhang; (II) Administrative support: L Zhou; (III) Provision of study materials or patients: Z Lin, Y Xu; (IV) Collection and assembly of data: Z Lin, Y Xu, L Guan; (V) Data analysis and interpretation: Z Lin; (VI) Manuscript writing: All authors; (VII) Final approval of manuscript: All authors.

[#]These authors contributed equally to this work.

Correspondence to: Luqian Zhou, PhD; Qingling Zhang, PhD. State Key Laboratory of Respiratory Disease, National Clinical Research Center for Respiratory Disease, Guangzhou Institute of Respiratory Health, First Affiliated Hospital of Guangzhou Medical University, 151 Yanjiangxi Road, Guangzhou 510120, China. Email: zhxl09@163.com; zqling68@hotmail.com.

Background: Chronic obstructive pulmonary disease (COPD) is a chronic respiratory disease characterized by incomplete reversible airway obstruction, with high mortality and disability rates, and smoking is the primary risk factor for COPD. Studies performed to date have confirmed that iron and ferroptosis play crucial roles in the development of cigarette smoke-induced COPD, but the exact mechanisms have not been fully elucidated.

Methods: The microarray datasets GSE10006, GSE11784, and GSE20257 were downloaded from the Gene Expression Omnibus (GEO) database to identify differentially expressed genes (DEGs) between COPD smokers and non-smokers airway epithelial. Protein-protein interaction (PPI) and hub gene networks were constructed using the STRING database and Cytoscape software. At the same time, the 3 datasets were screened for ferroptosis-related genes that were co-differentially expressed. The ferroptosis-related hub genes (FRHGs) that overlapped with the ferroptosis-related genes and hub genes were then identified. Next, the mRNA-miRNA network was constructed, and Gene Ontology (GO) annotation and Kyoto Encyclopedia of Genes and Genomes (KEGG) pathway enrichment analysis for target genes were performed. Finally, GSE19407, GSE994, and GSE27973 were used to evaluate the expression of hub genes.

Results: We identified 7 potential FRHGs (*NQO1*, *AKR1C3*, *AKR1C1*, *GPX2*, *TXNRD1*, *SRXN1*, *SLC7A11*), which showed good diagnostic properties. The molecular functions (MFs) of FRHGs mainly influence biological processes (BPs) responding to oxidative stress. Nrf2 pathways may be the key pathways regulating ferroptosis in cigarette smoke-induced COPD. Meanwhile, co-expressed mRNAs and miRNAs were selected to construct mRNA-miRNA interaction networks. Furthermore, based on the 7 FRHGs mentioned above, we found that benzoic acid showed high drug targeting relevance.

Conclusions: This work identified 7 FRHGs as potential biomarkers for the diagnosis and treatment of COPD and provided insights into the mechanisms of disease development in cigarette smoke-induced COPD at the transcriptome level.

Keywords: Chronic obstructive pulmonary disease (COPD); ferroptosis; cigarette; bioinformatics analysis

Submitted Feb 14, 2022. Accepted for publication Mar 16, 2022.

doi: 10.21037/atm-22-1009

View this article at: <https://dx.doi.org/10.21037/atm-22-1009>

Introduction

Chronic obstructive pulmonary disease (COPD) is a chronic respiratory disease characterized by incomplete and reversible airway obstruction, with high rates of mortality and disability (1). Patients with COPD are at higher risk of developing other diseases, such as lung cancer (2), than healthy individuals. Risk factors for COPD include genetic factors, smoking, and airway inflammation (3-5), with smoking being the primary risk factor. There is also growing evidence that the pathogenesis of COPD involves multiple biological functions, including cell proliferation, apoptosis, autophagy, and ferroptosis (6-9).

Ferroptosis is a novel form of regulated cell death discovered by Dixon *et al.* (10) in 2012. In contrast to other cell death modalities such as apoptosis, necrosis, and autophagy, it is mainly characterized by the iron-dependent accumulation of lipid peroxidation, which manifests as abnormal metabolism of intracellular lipid oxides catalyzed by excess iron ions, reactive oxygen species (ROS) production, and polyunsaturated fatty acid (PUFA) over-oxidation-mediated regulated cell death. Studies have shown that the onset and progression of many diseases are associated (11) with the ferroptosis pathway, including many respiratory diseases other than COPD, such as asthma (12) and acute lung injury (13). The study (14) has confirmed that iron and ferroptosis play critical roles in the development of COPD, but the exact mechanisms are not yet fully understood. Meanwhile, oxidative stress, caused by an imbalance between oxidants and antioxidants, is thought to underlie COPD after exposure to smoking. Cigarette smoke increases the respiratory tract's burden of oxidants, which are contained directly in cigarette smoke or produced by inflammatory cells, depleting antioxidant defences and injuring lung cells (15). Exposure to cigarette smoke increases cell lysis and epithelial permeability, effects that can be inhibited by antioxidants (16).

Direct measurements of the distribution of lower airway resistance (17-19) showed that small airways (internal diameter <2 mm) are the primary site of obstruction in patients with COPD. The airway epithelium is the first line of defence upon exposure of the respiratory system to cigarette smoke. High-throughput sequencing has evolved rapidly over the past decade and advances in gene microarray expression analysis have greatly facilitated the exploration of key genes in the pathobiology of COPD. Most of the current bioinformatics-related studies (20,21)

in COPD have focused on peripheral blood samples, and they (20,21) have identified many differentially expressed genes based on mRNA expression profiles. However, these differentially expressed genes cannot fully explain the pathogenesis of COPD, because peripheral blood does not directly reflect the pathological changes in COPD. At the same time, there is a gap in the study of ferroptosis at the transcriptome level in airway epithelial tissues. The present study is the first to focus innovative attention on exploring the relationship between airway epithelial tissue and ferroptosis-related hub genes of cigarette smoke-induced chronic obstructive pulmonary disease. We have a deep conviction that microarray datasets from airway epithelial tissue may reflect COPD pathology more accurately and directly than those from peripheral blood.

In this study, we analyzed 3 COPD airway epithelial cell microarray datasets from the Gene Expression Omnibus (GEO) database for differentially expressed genes (DEGs) in COPD airway epithelial cells and further screened genes that were differentially expressed in all 3 datasets as target genes. Then, related protein-protein interaction (PPI) networks were constructed, and genes with the top 5% of interaction scores were screened as hub genes using the MCC algorithm of the Cytohubba plugin in Cytoscape software. At the same time, the 3 datasets were screened for ferroptosis-related genes that were co-differentially expressed. The ferroptosis-related hub genes (FRHGs) that overlapped with the ferroptosis-related genes and hub genes were then identified. The FRHGs were further subjected to Gene Ontology (GO) and Kyoto Encyclopedia of Genes and Genomes (KEGG) analyses. The expression of the above genes was then evaluated in the GSE19407 dataset, and an mRNA-miRNA network was constructed to explore the potential regulatory effects of miRNAs on FRHGs in COPD. Healthy smokers as a source of data in the microarray dataset GSE19407 were further analyzed and compared with healthy non-smokers to investigate whether smoking causes a difference in the expression of the above genes. The effect of smoking on differentially expressed ferroptosis-related genes was further validated in microarray dataset GSE994. Finally, to definitively identify cigarette smoke as an inducer of the differential expression of FRHGs in epithelial cells, the GSE27973 dataset was used for validation. We present the following article in accordance with the STREGA reporting checklist (available at <https://atm.amegroups.com/article/view/10.21037/atm-22-1009/rc>).

Table 1 Details of GEO COPD data

Accession	Platform	Sample	Non-smoker	Former smoker	Smoker	COPD	Gene
GSE10006	GPL570	Airway epithelial	13	–	–	14	<i>mRNA</i>
GSE11784	GPL570	Airway epithelial	52	–	–	21	<i>mRNA</i>
GSE20257	GPL570	Airway epithelial	42	–	–	23	<i>mRNA</i>
GSE19407	GPL570	Airway epithelial	36	–	50	22	<i>mRNA</i>
GSE994	GPL96	Airway epithelial	23	18	–	–	<i>mRNA</i>
GSE27973	GPL570	Primary epithelial cells	4	–	–	–	<i>mRNA</i>

GEO, Gene Expression Omnibus; COPD, chronic obstructive pulmonary disease.

Methods

Data acquisition

A total of 214 ferroptosis-related genes were obtained from the FerrDb database (<http://www.zhounan.org/ferrdb/>). The mRNA expression profile datasets GSE10006, GSE11784, GSE20257, GSE19407, GSE994, and GSE27973 were downloaded from the GEO database (<https://www.ncbi.nlm.nih.gov/geo/>) in the data format MINiML. The datasets GSE10006, GSE11784, GSE20257, GSE19407, and GSE27973 are located on the GPL570 platform [(HG-U133_Plus_2) Affymetrix Human Genome U133 Plus 2.0 Array], while GSE994 is located on the GPL96 platform [(HG-U133A) Affymetrix Human Genome U133A Array]. Airway epithelial samples from GSE10006, GSE11784, and GSE20257 were included for screening DEGs and FRHGs. Meanwhile, GSE19407 was used for validation of the target hub genes and for probing the effect of smoking on differentially expressed FRHGs. GSE994 included airway epithelial samples to investigate the effect of smoking cessation on differentially expressed FRHGs. GSE27973 contained data from 4 samples of human primary epithelial cells provided by healthy donors which were incubated with cigarette smoke extract (CSE) for 24 h to further probe the effect of cigarette smoke on differentially expressed FRHGs in airway epithelial cells. After identity document (ID) transformation, when multiple probes corresponded to 1 gene, the average expression value was taken as the gene expression value. Raw data were log₂-transformed and quantile-normalized prior to analysis.

Detailed information of the 3 datasets is shown in *Table 1*, and a flow chart of the study design is shown in *Figure 1*.

Analysis of differential gene expression

The normalized expression matrix of the microarray data was downloaded from the 4 datasets and represented by a box line plot (plotted by boxplot). The probes were then annotated with the annotation file in the dataset. Reproducibility of the data was verified by principal component analysis (PCA), and PCA plots were plotted using the R package ggord.

Genes with an adjusted P value less than 0.05 and absolute fold change (FC) greater than 1 were considered as DEGs using the ‘limma’ package of R software (22). Heat map, volcano maps, and box line plots were created using the ‘heatmap’ and ‘ggplot2’ packages (version 3.3.3) of R software (version 3.6.3) (23).

PPI analysis and correlation analysis of DEGs

The PPI network of DEGs was analyzed using the STRING database (<https://string-db.org/>). The STRING analysis data were imported using Cytoscape software (version 3.8.1), and the genes with the top 5% of scores were tagged as hub genes using the MCC algorithm of the Cytohubba plugin in Cytoscape. Using the human ferroptosis database to match the hub genes, those that overlapped with the ferroptosis-related genes and hub genes were then identified.

Construction of an mRNA-miRNA regulatory network

Interactions between differentially expressed miRNAs and differentially expressed mRNAs were predicted using the

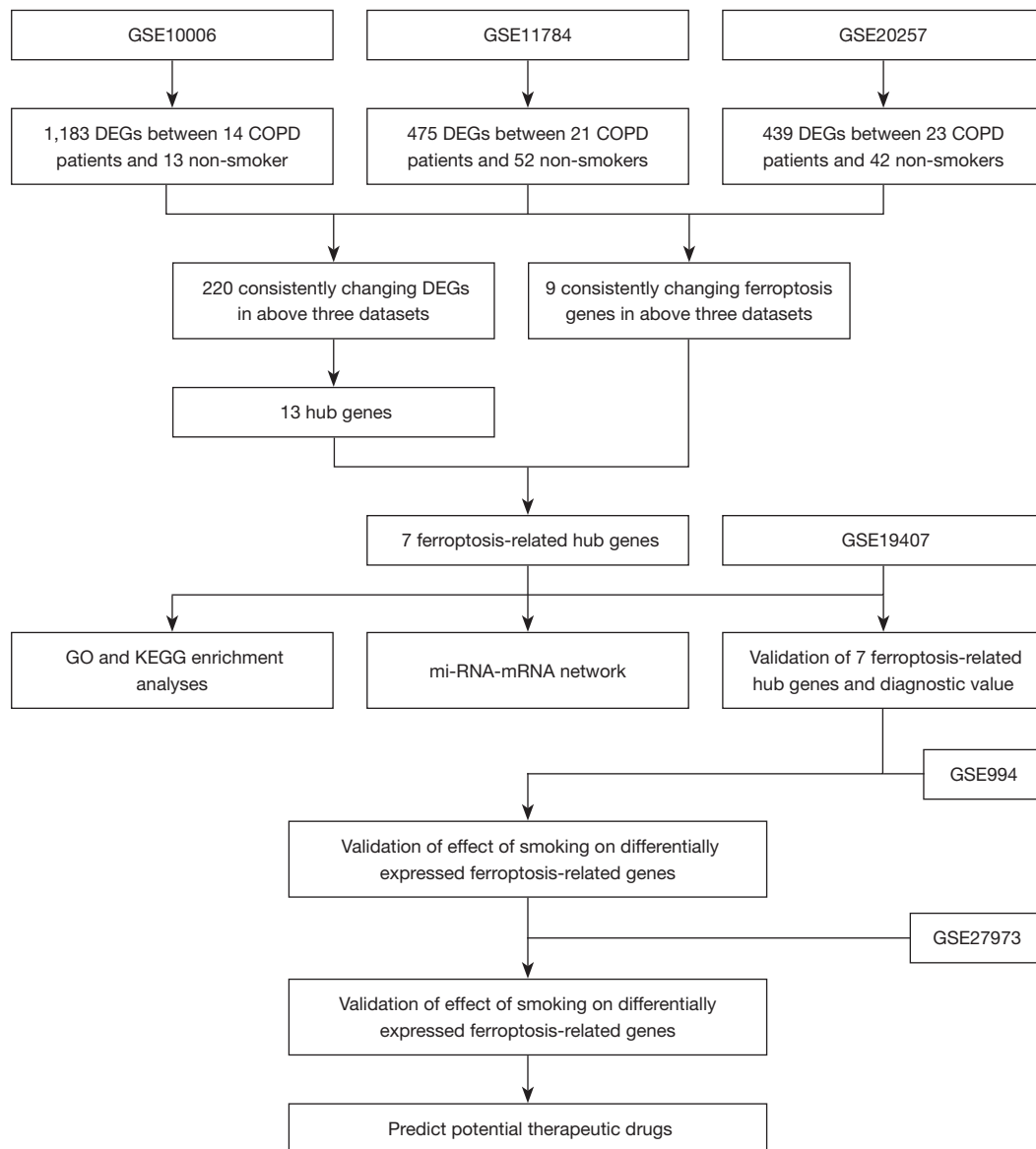


Figure 1 The overall protocol of this study. DEGs, differentially expressed genes; COPD, chronic obstructive pulmonary disease; GO, Gene Ontology; KEGG, Kyoto Encyclopedia of Genes and Genomes.

miRNet database (predicted at <https://www.mirnet.ca/>). Then, the mRNA-miRNA regulatory network was established to describe the interactions between mRNAs and miRNAs as potential targets in COPD airway epithelial cells. Cytoscape software was used to visualize the regulatory network.

GO and KEGG pathway enrichment analyses of genes

The ClusterProfiler package in R was used to conduct GO and KEGG pathway analysis on FRHGs. The species was

limited to Homo sapiens, and the “adjusted P value (from the Benjamini-Hochberg method), 0.05” was considered statistically significant. The GO terms included these 3 criteria: molecular function (MF), cellular component (CC), and biological process (BP).

Gene set enrichment analysis (GSEA)

To explore biological signaling pathways, GSEA was performed. The KEGG pathway with significant

enrichment results was demonstrated based on net enrichment score (NES), gene ratio, and P value. $|\text{NES}| > 1$ and FDR $q < 0.25$ were considered to represent significant enrichment.

Validation of ferroptosis hub genes

Receiver operating characteristic (ROC) curve analysis was performed using HiPlot software (version 0.1.0) to determine the sensitivity and specificity of target genes. Multigene ROC analysis was performed based on the predicted probability of multiple genes contributing to the outcome in each sample calculated by binary logistic regression using SPSS version 22.0. Results were quantified by the area under the ROC curve (AUC), and genes with AUC > 0.6 were considered diagnostic.

Potential therapeutic drug prediction

Protein-drug interaction data from the DSigDB database (<http://tanlab.ucdenver.edu/DSigDB>) were used to predict potential therapeutic agents for COPD, with FDR < 0.05 and composite score $> 5,000$ used as thresholds.

Ethical statement

The study was conducted in accordance with the Declaration of Helsinki (as revised in 2013).

Statistical analysis

We used GraphPad Prism 5 and version 3.6.3 of R software for statistical analysis. Data were expressed as mean \pm standard deviation and unpaired Student's *t*-test was used for comparison between groups. A P value less than 0.05 is statistically significant.

Results

Ferroptosis hub gene screening in COPD small airway epithelial cells

The expression matrices of the 4 datasets GSE10006, GSE11784, GSE20257, and GSE19407 were normalized, and the distribution trends of the box plots were basically straight lines (Figure 2A-2D). To assess the repeatability of the data within the group, PCA of the 4 datasets was performed in this study, and the results showed good

repeatability of the data (Figure 2E-2H).

After screening with the threshold of an adjusted $|\log_2(\text{FC})| > 1$ and P value < 0.05 , 1,183 DEGs (988 upregulated and 195 downregulated) were identified in the GSE10006 dataset, 475 DEGs (317 upregulated and 158 downregulated) were identified in the GSE11784 dataset, and 439 DEGs (291 upregulated and 148 downregulated) were identified in the GSE20257 dataset. The volcano plots of DEGs in the above 3 datasets are shown in Figure 3A-3C, and detailed information regarding the DEGs is listed in (<https://cdn.amegroups.com/static/public/atm-22-1009-1.docx>). Venn plots were also created (Figure 3D), which showed that 220 genes were commonly differentially expressed among the 3 datasets, of which 157 were upregulated and 63 were downregulated (Table S1).

The PPI network (Figure 3E) was also generated by determining the interactions among the DEGs obtained above. The STRING analysis data were imported using Cytoscape software (version 3.8.1), and the genes with the top 5% of scores were tagged as hub genes. Thirteen hub genes were finally identified, namely, *NQO1*, *AKR1C3*, *AKR1C1*, *ALDH3A1*, *CYP1A1*, *GPX2*, *TXNRD1*, *CBR1*, *AKR1B10*, *CBR3*, *SRXN1*, *CYP1B1*, and *SLC7A11* (Figure 3F).

We next analyzed the expression of 214 ferroptosis-related genes in the 3 datasets, and ferroptosis-related genes were identified using the criteria of adjusted $|\log_2(\text{FC})| > 1$ and P value < 0.05 (Table S2). Venn diagram analysis of the 3 datasets identified the following genes which were differentially expressed in ferroptosis: *GPX2*, *SLC7A11*, *DUOX2*, *AKR1C3*, *NQO1*, *AKR1C1*, *SRXN1*, *TXNRD1*, and *SLC2A3* (Figure 3G). Interestingly, many of these genes overlapped with the hub genes obtained as described above, namely, *NQO1*, *AKR1C3*, *AKR1C1*, *GPX2*, *TXNRD1*, *SRXN1*, and *SLC7A11*. We finally identified *NQO1*, *AKR1C3*, *AKR1C1*, *GPX2*, *TXNRD1*, *SRXN1*, and *SLC7A11* as both hub genes and genes differentially expressed in ferroptosis (Figure 3H).

Construction of the gene network and GO/KEGG enrichment analyses of FRHGs

We used the miRNet tool to predict target miRNAs of hub genes. Finally, we obtained 281 target miRNAs of 7 specifically expressed FRHGs and determined 359 mRNA-miRNA pairs. According to the prediction results, a co-expressed network of mRNAs and miRNAs, which comprised 288 nodes and 359 edges, was constructed by

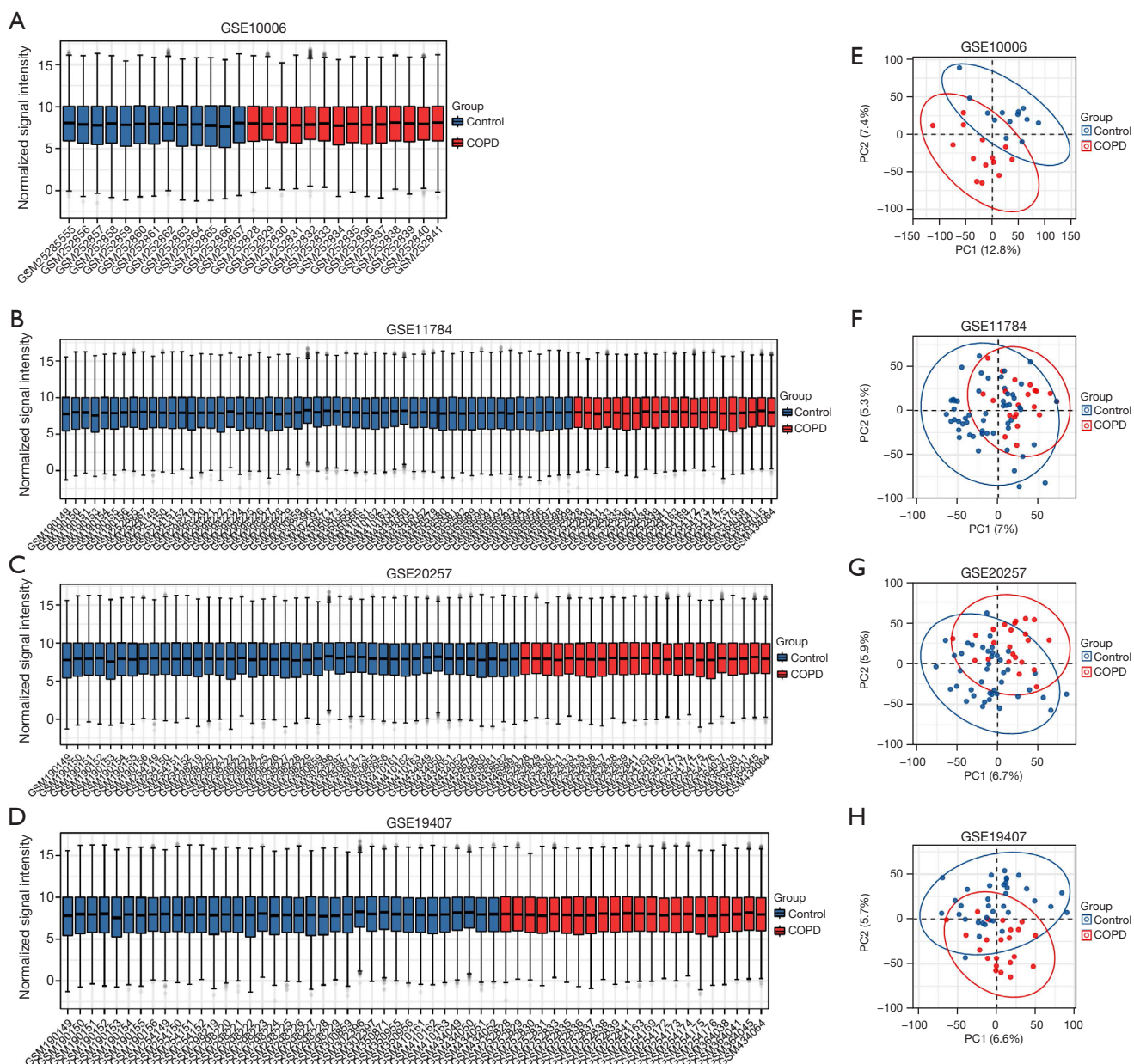


Figure 2 Normalized expression matrices (A-D) and PCA diagrams (E-H) of the GSE10006, GSE11784, GSE20257, and GSE19407 datasets. PCA, principal component analysis.

Cytoscape (Figure 4A). There were 184 miRNAs regulating SLC7A11, 91 miRNAs regulating TXNRD1, 25 miRNAs regulating SRXN1, 24 miRNAs regulating AKR1C3, 21 miRNAs regulating NQO1, 8 miRNAs regulating GPX2, and 6 miRNAs regulating AKR1C1 (Table S3).

We further searched the PubMed database (<https://pubmed.ncbi.nlm.nih.gov/>) for literature related to miRNAs and COPD airway epithelium to screen for

those overlapping with the above 281 miRNAs, excluding nonhuman specimen studies and studies without validation. This identified a total of 19 miRNAs: hsa-miR-130a-3p (24), hsa-miR-21 (25), hsa-miR-223-5p (26), hsa-miR-494-3p (27), miR-146a-5p (28), miR-221-3p (29), hsa-miR-92a-3p (29), miR-483-5p (30), hsa-miR-218-5p (31), miR-24-3p (32), miR-218 (33), miR-195 (34), hsa-miR-181c-5p (35), miR-16 (36), miR-222 (36), hsa-miR-29b-3p (37), hsa-miR-200c-

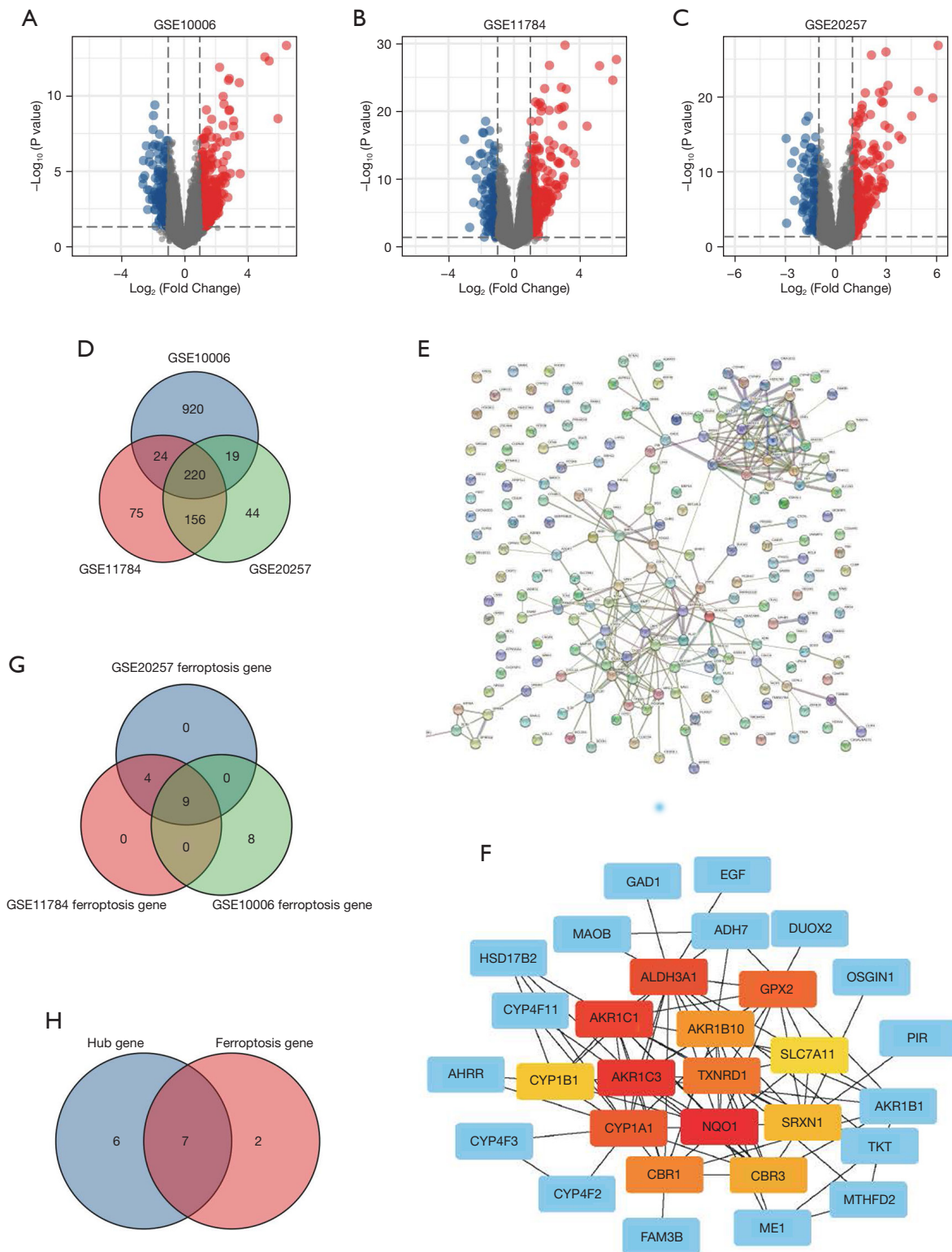
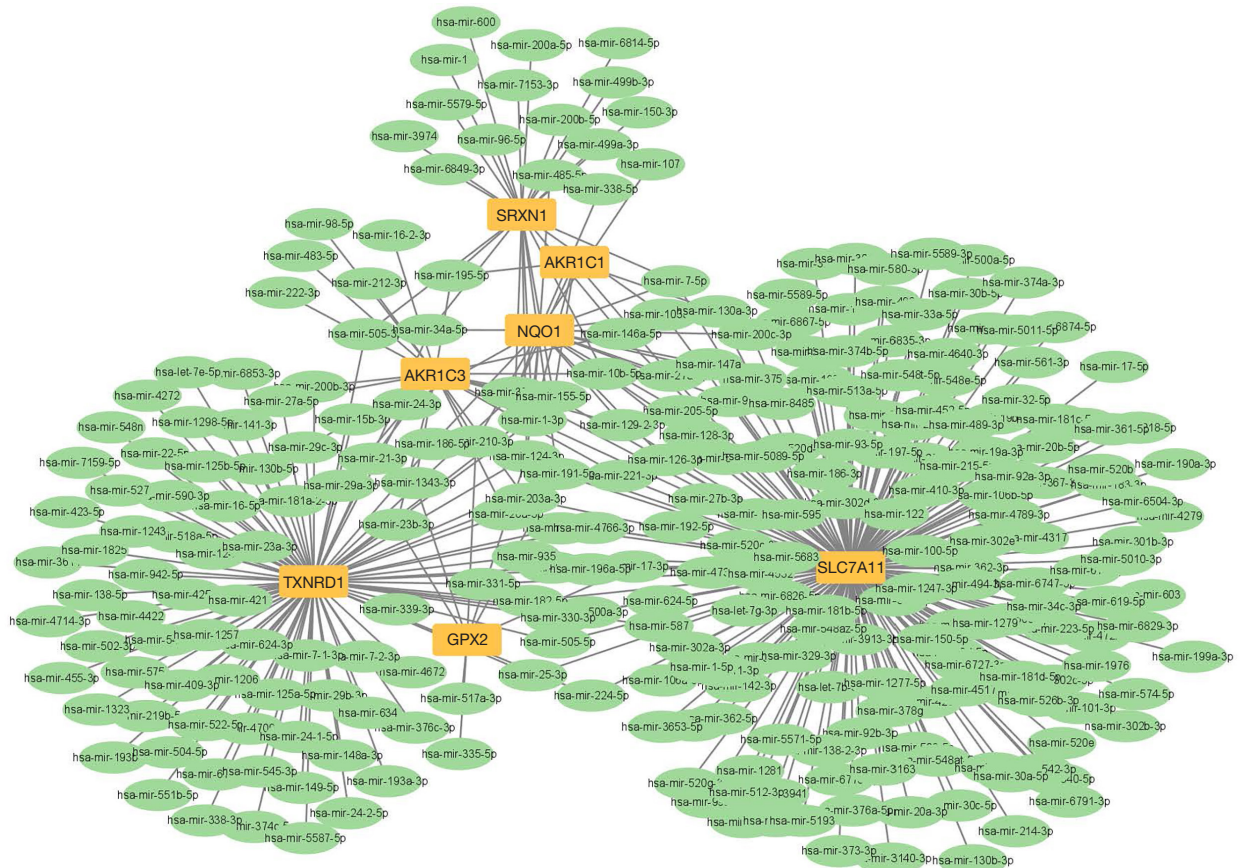
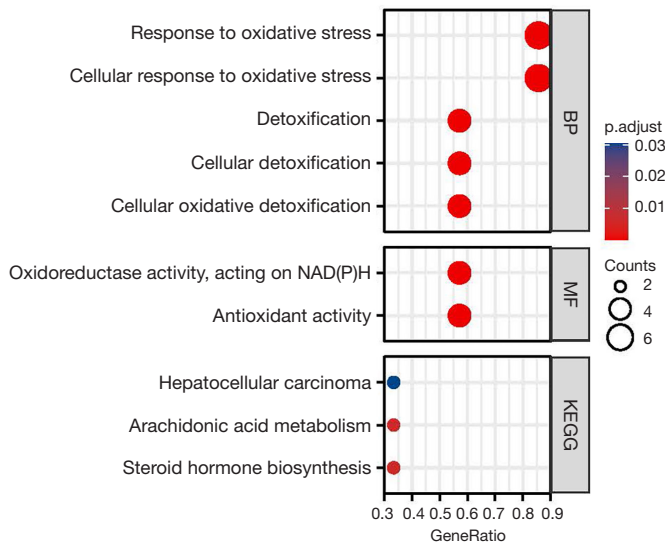


Figure 3 Differentially expressed genes and ferroptosis-related hub genes of the GSE10006, GSE11784 and GSE20257 datasets. (A-C) The volcano plots of GSE10006, GSE11784, and GSE20257; (D) differential genes in the 3 datasets; (E) STRING; (F) hub genes; (G) ferroptosis-related genes; (H) ferroptosis-related hub genes.

A



B



C

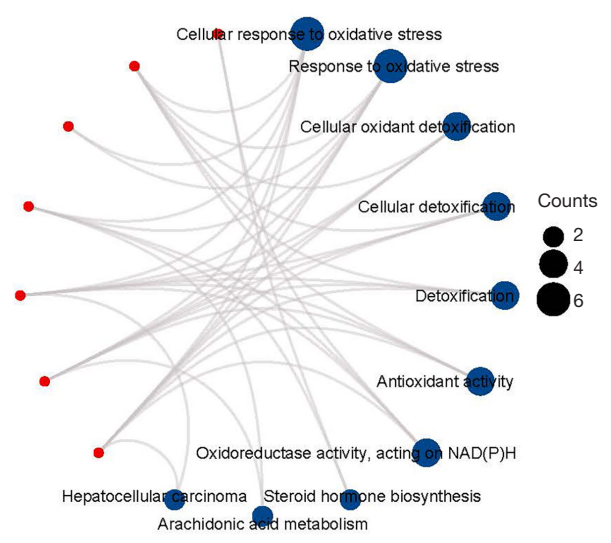


Figure 4 mRNA-miRNA regulatory network and GO/KEGG of ferroptosis-related hub genes. (A) mRNA-miRNA regulatory network; (B,C) GO/KEGG categories and pathways. BP, biological process; MF, molecular function; GO, Gene Ontology; KEGG, Kyoto Encyclopedia of Genes and Genomes.

3p (38), hsa-miR-361-5p (39), and miR-146a (40).

GO and KEGG enrichment analyses were performed on 7 differentially expressed ferroptosis hub genes. The results showed that the GO categories with the greatest enrichment were cellular response to oxidative stress, response to oxidative stress, cellular oxidant detoxification, cellular detoxification, detoxification, antioxidant activity, oxidoreductase activity, acting on NAD(P)H, and other processes. In the KEGG enrichment analysis, the DEGs were particularly involved in metabolic processes such as steroid hormone biosynthesis, arachidonic acid metabolism, and hepatocellular carcinoma (Figure 4B,4C).

GSE19407 confirms the expression and diagnostic value of the FRHGs

The expression of the screened target genes was tested with GSE19407. The results showed that the expression of the 7 ferroptosis-related hub genes (*NQO1*, *AKR1C3*, *AKR1C1*, *GPX2*, *TXNRD1*, *SRXN1*, *SLC7A11*) that were differentially expressed between COPD-affected smokers and non-smoking healthy subjects was consistent with the predictions (Figure 5A-5G). Then, GSEA was performed to identify the functional enrichment in COPD-affected smokers and non-smoking healthy individuals, with the results then being compared with the 7 genes obtained as described above. The results showed that most genes were located in WP_NRF2_PATHWAY (NES =2.151; P.adjust =0.025; FDR =0.024) and WP_NUCLEAR_RECEPTORS_METAPATHWAY (NES =2.067; P.adjust =0.025; FDR =0.024) signaling pathway enrichment (Figure 5H,5I; <https://cdn.amegroups.com/static/public/atm-22-1009-2.xlsx>). We created ROC curves using data from COPD-affected smokers versus healthy subjects. The results showed that these 7 genes have significant value for diagnosing COPD in smokers. The AUC of the variable *SRXN1* was 0.823 (95% CI: 0.744–0.902), that of *SLC7A11* was 0.817 (95% CI: 0.732–0.903), that of *GPX2* was 0.799 (95% CI: 0.710–0.887), that of *NQO1* was 0.789 (95% CI: 0.702–0.875), that of *TXNRD1* was 0.765 (95% CI: 0.667–0.863), that of *AKR1C3* was 0.757 (95% CI: 0.665–0.849), and that of *AKR1C1* was 0.732 (95% CI: 0.636–0.828) (Figure 5J-5P).

Differential expression analysis of genes related to smoking and ferroptosis

Cigarette smoke is the primary causative agent of COPD,

and it has also been shown that it can cause ferroptosis in the airway epithelium. We further investigated the effect of smoking on the expression of FRHGs using GSE19407 (including non-smoker, smoker, and COPD samples). Two-way comparisons of COPD versus non-smokers, COPD versus smokers, and non-smokers versus smokers were performed for GSE19407. The 3 datasets were normalized, and the distribution trends of the box plots were basically straight lines (Figure 6A-6C). To assess the repeatability of the data within the group, PCA of the 3 datasets was performed in this study, and the results showed that the repeatability of the data was good (Figure 6D-6F).

The 3 datasets were analyzed and the volcano plots of FRHGs in the above 3 datasets are shown in Figure 7A-7C. The plots showed that there was a large difference in the expression of ferroptosis-related genes in non-smoking healthy individuals compared with that in COPD patients, with the ferroptosis genes being upregulated in COPD patients. There was a difference in the expression of ferroptosis-related genes in non-smoking healthy individuals compared with that in healthy smokers, but not as large as in comparison with COPD patients. There was also a small difference in the expression of ferroptosis-related genes in COPD patients compared with that in healthy smokers (Figure 7D-7J).

Through further analysis, it was shown that smokers had significant upregulation of *NQO1*, *AKR1C3*, *AKR1C1*, *GPX2*, *TXNRD1*, *SRXN1*, and *SLC7A11* compared with non-smokers, and after smoking cessation, the expression of this fraction of genes returned to levels consistent with those in non-smokers (Figure 7K,7L). To further confirm cigarette smoke as an inducer of the differential expression of genes associated with ferroptosis in airway epithelial cells, the GSE27973 dataset was used for validation. The volcano plots and heat map of GSE27973 showed that *NQO1*, *TXNRD1*, *GPX2*, *AKR1C3*, and *AKR1C1* were significantly upregulated, while *SRXN1* and *SLC7A11* were upregulated, albeit not significantly (Figure 7M,7N). Therefore, it can be concluded that cigarette smoke can cause the upregulation of the ferroptosis-related genes *NQO1*, *AKR1C3*, *AKR1C1*, *GPX2*, *TXNRD1*, *SRXN1*, and *SLC7A11* in small airway epithelial cells.

Targeted drug prediction

We used the DSigDB database to predict potential target drugs associated with key genes that may be useful for treating COPD by modulating ferroptosis. A total of 581

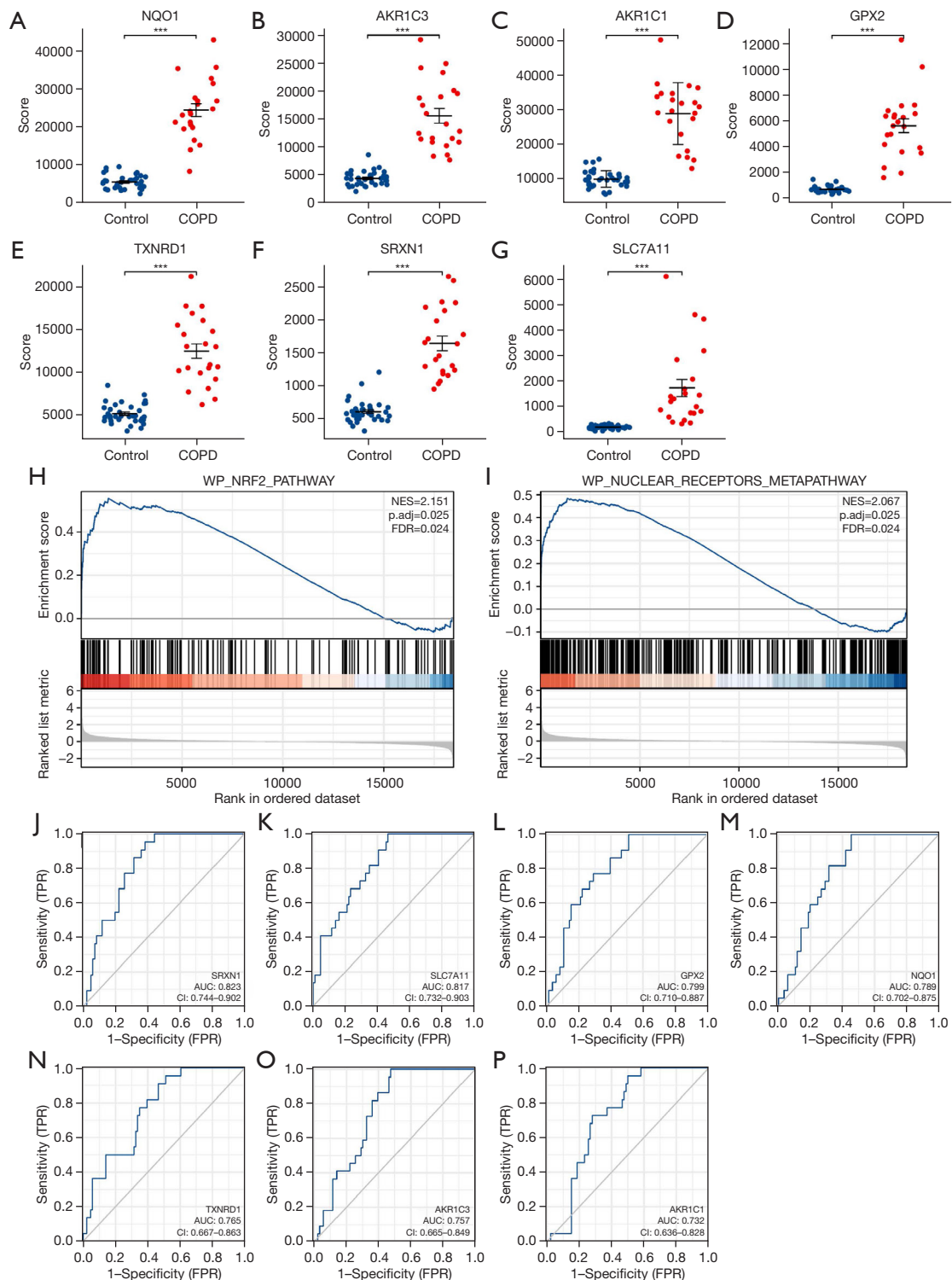


Figure 5 Comparison of the expression and diagnostic ROC curves of 7 ferroptosis-related hub genes. (A-G) Comparison of the expression of 7 ferroptosis-related hub genes in COPD and healthy samples; (H,I) signaling pathways where the 7 ferroptosis-related hub genes are predominant in COPD and healthy samples; (J-P) diagnostic ROC curves of 7 ferroptosis-related hub genes in COPD and healthy samples. ***, $P < 0.001$. COPD, chronic obstructive pulmonary disease; ROC, receiver operating characteristic; TPR, true positive rate; FPR, false positive rate.

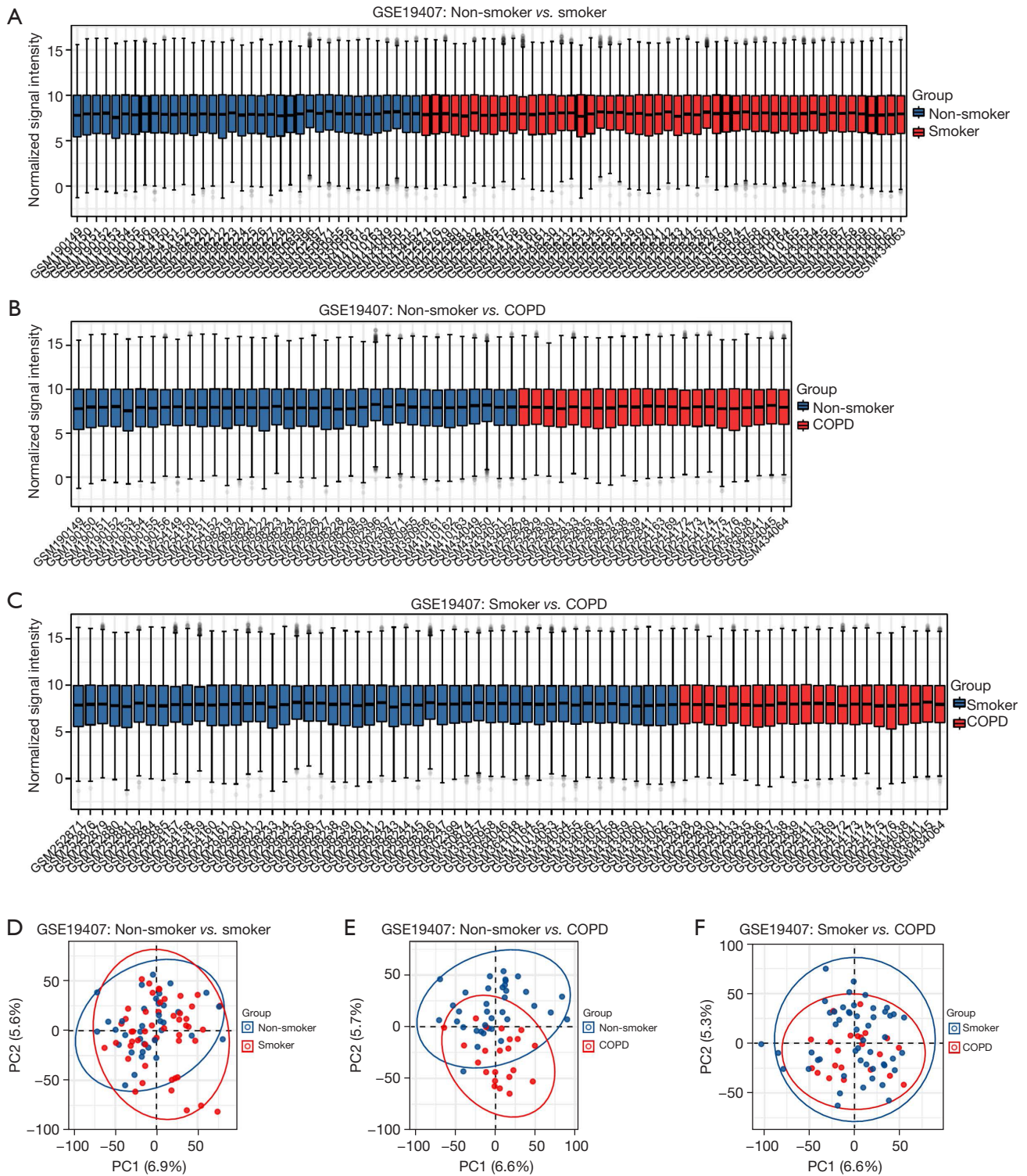


Figure 6 Normalized expression matrices and principal component analysis of 3 datasets (COPD and non-smoker/COPD and smoker/non-smoker and smoker). COPD, chronic obstructive pulmonary disease.

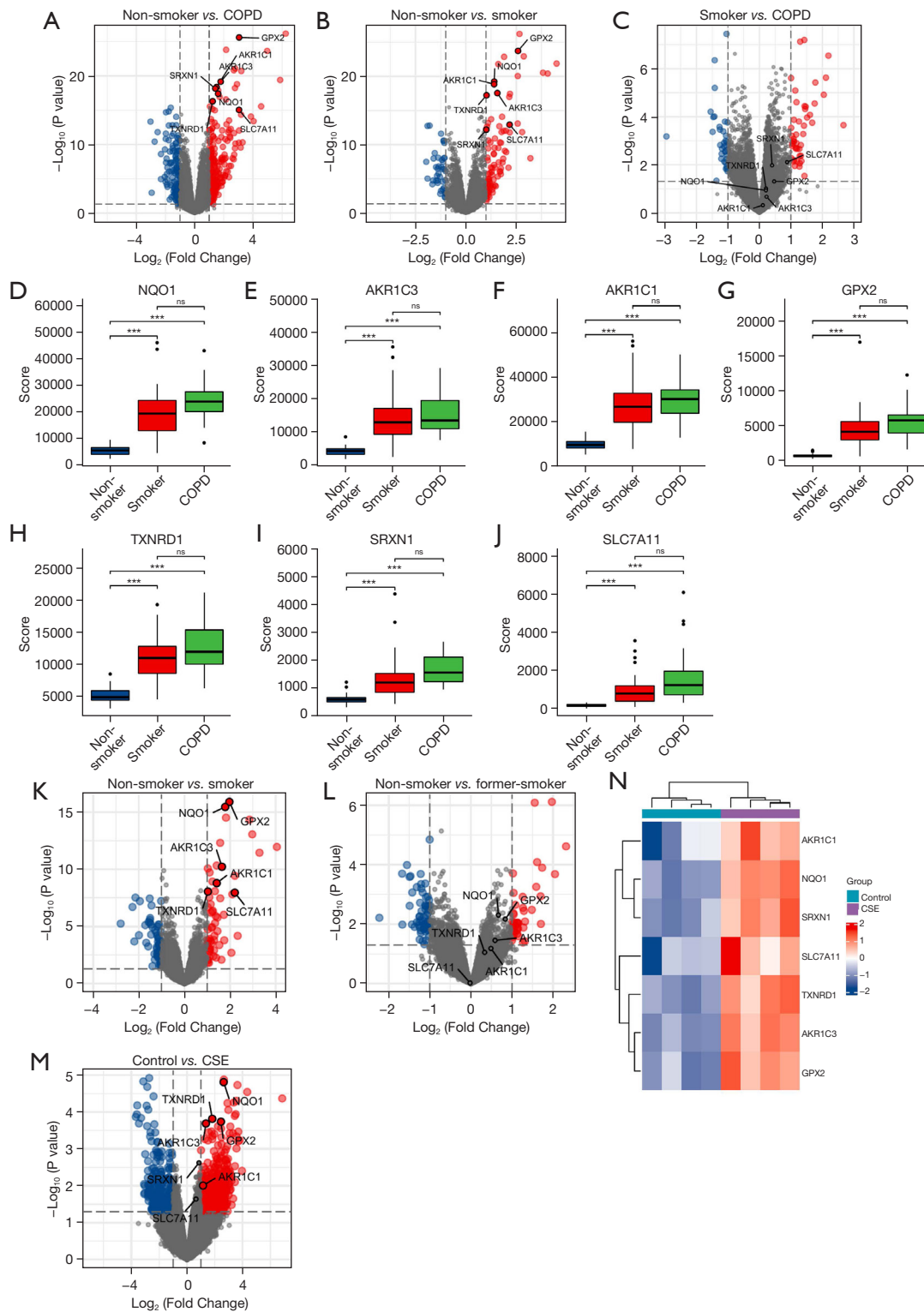


Figure 7 Differential expression analysis of genes related to smoking and ferroptosis. (A-C) Volcano plots of ferroptosis-related hub genes in the 3 datasets; (D-J) differences of ferroptosis-related hub genes in the 3 datasets; (K,L) volcano plots of before and after quitting smoking; (M,N) the volcano plots and heat map of GSE27973. ***, $P < 0.001$; ns, no significance. COPD, chronic obstructive pulmonary disease; CSE, cigarette smoke extract.

Table 2 Top 10 predicted target drugs

Index	Name	P value	Odds ratio	Combined score
1	Glycidamide CTD 00002776	1.62E-16	139,202	5,061,164.541
2	Arsenous acid CTD 00000922	4.40E-09	131,019	2,520,968.068
3	Hydrogen peroxide CTD 00006118	7.56E-07	121,289	1,709,522.752
4	Tetradioxin CTD 00006848	8.39E-06	113,624	1,328,140.359
5	Acetaminophen CTD 00005295	1.61E-05	111,055	1,225,803.307
6	Estradiol CTD 00005920	2.24E-05	109,648	1,173,815.852
7	Benzo[a]pyrene CTD 00005488	2.58E-05	109,032	1,151,876.014
8	HEXANE CTD 00001239	3.34E-14	2,628	81,550.7241
9	Benzoic acid CTD 00007316	6.35E-14	2,269	68,964.25003
10	Lactic acid CTD 00007283	6.35E-14	2,269	68,964.25003

target drugs were finally predicted, and the combined scores and corresponding target genes are listed in (<https://cdn.amegroups.com/static/public/atm-22-1009-3.xlsx>). The top 10 predicted target drugs according to the combined scores are shown in *Table 2*. Among these compounds, a study has shown that drugs containing arsenous acid can treat osteoporosis (41). Most notable among these is benzoic acid, for which there is now scientific evidence supporting its effectiveness as a novel therapeutic compound for treating COPD (42).

Discussion

In recent years, the diagnosis and treatment of COPD have been increasingly studied, but the prognosis of COPD patients remains poor due to the limited understanding of the pathogenesis of this disease and the absence of specific drugs. In this study, we constructed a PPI network by analyzing 3 COPD airway epithelial cell microarray datasets (GSE10006, GSE11784, and GSE20257) from the GEO database and screened for DEGs among the 3 datasets. Meanwhile, 13 hub genes and 9 ferroptosis genes with associated differential expression were screened, and then we finally obtained 7 FRHGs, namely, *NQO1*, *AKR1C3*, *AKR1C1*, *GPX2*, *TXNRD1*, *SRXN1*, and *SLC7A11*. These 7 genes were further screened using the miRNet tool to combine the results of differentially expressed FRHGs with the interaction network of miRNAs, providing a total of 281 miRNAs and 359 mRNA-miRNA pairs. Then, using GO and KEGG pathway analyses, we found that the most enriched GO categories were cellular response

to oxidative stress, response to oxidative stress, cellular oxidant detoxification, cellular detoxification, detoxification, antioxidant activity, oxidoreductase activity, acting on NAD(P)H, and other processes. In the KEGG enrichment analysis, the DEGs were mainly involved in metabolic processes such as steroid hormone biosynthesis, arachidonic acid metabolism, and hepatocellular carcinoma.

In the validation step, further analysis of the microarray dataset GSE19407 revealed that smoking does indeed lead to the upregulation of FRHG expression, and these genes are more upregulated upon the transition from healthy smokers to COPD patients. In addition, in the microarray dataset GSE994, it was found that after smoking cessation, the expression levels of these genes were restored to those in healthy never-smokers. Finally, to confirm cigarette smoke as an inducer of the differential expression of FRHGs in airway epithelial cells, the GSE27973 dataset was used for validation. This showed that the expression of the FRHGs was upregulated in human primary epithelial cell samples provided by healthy donors incubated with CSE for 24 h. GSEA was also performed in this study to identify functional enrichment in COPD smokers and non-smoking healthy individuals. The results showed that 5 genes (*GPX2*, *SLC7A11*, *NQO1*, *SRXN1*, *TXNRD1*) were expressed in WP_NRF2_PATHWAY and WP_NUCLEAR_RECEPTORS_METAPATHWAY.

Among the 7 FRHGs, *SLC7A11*, *AKR1C3*, *NQO1*, and *AKR1C1* are ferroptosis suppressor genes (43), while *GPX2*, *SRXN1*, and *TXNRD1* are ferroptosis marker genes (43). Among these, *TXNRD1*, *AKR1C1*, *AKR1C3*, and *NQO1* are ROS detoxification enzymes (43). Moreover,

GPX2 is the major cigarette smoke-induced isoform of glutathione peroxidase (GPX) in the lung and is regulated by nuclear factor E2-related factor 2 (Nrf2), whose main role is to scavenge hydrogen peroxide or organic hydroperoxides, thereby protecting biological membranes and cellular components from oxidative stress (44). Tian *et al.* demonstrated that the knockdown of GPX2 partially reversed the increase in lipid ROS and iron concentration induced by erastin, which supports the potential role of GPX2 as a driver of ferroptosis (45). SLC7A11 is a classical modulator of ferroptosis-mediating proteins, and a study has suggested that SLC7A11-mediated cystine uptake plays a key role in inhibiting oxidative responses and maintaining cell survival under oxidative stress conditions (46). Meanwhile, NQO1 is a multifunctional antioxidant enzyme that plays a key role in protecting cells from oxidative damage through proteasomal degradation, exogenous detoxification, p53 regulation, superoxide scavenging and maintenance of endogenous antioxidants (47). In addition, AKR1C1-3 have been shown to be involved in the detoxification of toxic lipid metabolites (e.g., 4-hydroxynonenal) produced downstream of the oxidation of various polyunsaturated fatty acid substances (48). SRXN1 is an endogenous antioxidant that has been shown to prevent exogenous compound-induced oxidative stress *in vitro* and *in vivo* (49). TXNRD1 encodes a protein that belongs to the pyridine nucleotide-disulfide oxidoreductase family, and this protein is a member of the thioredoxin (Trx) system, which plays a key role in redox homeostasis (50). Notably, many of the above genes have been reported in cancer biology, but none have been previously shown to be associated with COPD, so further studies are needed to investigate their roles in this disease.

Further searches of the PubMed database for literature related to miRNAs and COPD airway epithelium, excluding nonhuman specimen studies and studies without validation, identified a total of 19 miRNAs. Among these, miR-130a, for example, has a pathogenic role in cigarette smoke-induced COPD and regulates Wnt/ β -catenin signaling by targeting Wnt1 (24). Inhibition of miR-494-3p has been reported to attenuate oxidative stress-induced cellular senescence and inflammation in primary epithelial cells from COPD patients (27). Significant downregulation of miR-483-5p in COPD samples abrogated the transforming growth factor- β (TGF- β)-mediated reduction in cell proliferation and increase in α -smooth muscle actin (α -SMA) and fibronectin expression in the lung epithelial and lung fibroblast cell lines BEAS-2B and HFL1 (30). Although

many studies related to COPD miRNAs have been performed, there is a gap in research related to ferroptosis, which requires more in-depth studies.

The NRF2 signalling pathway plays a key role in reducing lipid peroxidation and ferroptosis. Nrf2 is a key regulator required for the maintenance of oxidative homeostasis in cells and is activated under conditions of high oxidative stress (51). Nrf2 has several target genes, including intracellular redox homeostasis proteins such as heme oxygenase-1 (HO-1), NQO1, GPX, and SLC7A11 (52). These downstream factors play a crucial role in cellular defence mechanisms. Nrf2 directly or indirectly regulates many genes involved in the regulation of ferroptosis (53). Downregulation of TXNRD1 and SRXN1, important signalling molecules in the NRF2 signalling pathway, can also make cells more susceptible to ferroptosis (54). In addition, Nrf2 can induce ferroptosis by activating and upregulating downstream AKR1C1 and AKR1C3 (55). It has also been suggested that the severity of COPD and the development of respiratory failure may be related to the haplotype of the Nrf2 gene promoter (56). Consistent with these findings, Nrf2-deficient mice are more susceptible to cigarette smoke and develop more severe emphysema and apoptosis, along with inhibited antioxidant enzyme activity (57). These findings, together with the results of the present study, demonstrate that the imbalance in Nrf2 signalling pathway leads to an imbalance in antioxidant homeostasis and lipid peroxidation homeostasis, which in turn leads to the regulation of ferroptosis in epithelial cells and increases the risk of emphysema, ultimately accelerating the progression of chronic obstructive pulmonary disease.

Respiratory diseases are often characterised by epithelial injury, airway inflammation, defective tissue repair and airway remodelling, and COPD is no exception. Airway epithelial cells are key effectors of lung homeostasis and host defence. Epithelial cells are therefore essential in restoring homeostasis *in vivo*, coordinating inflammation regression and initiating tissue repair (58). In conjunction with the findings of this study, ferroptosis-regulated genes associated with the inhibition of ferroptosis occurrence in airway epithelial cells may be candidate targets for the treatment of COPD. In the meantime, the exploration of effective targeted therapies based on genes that play key roles in the pathology of this disease has been a focus of researchers. Based on the identified ferroptosis hub genes, we predicted several potential targeting agents, particularly benzoic acid. All-trans retinoic acid (ATRA) was shown to be useful for alveolar repair in COPD (59). Benzoic acid is

a derivative of ATRA but is more stable (59). In addition, lipocalin-deficient mice are a novel COPD model. This mouse model has more symptoms which are similar to human COPD than the classic mouse model of elastase-induced emphysema. It exhibits systemic symptoms associated with COPD, such as emphysema, bone loss, and reduced fat mass (60). The use of benzoic acid in the lipocalin-deficient COPD mouse model improved alveolar regeneration, suggesting the value of benzoic acid as a new therapeutic agent for COPD. Taking these previous findings together with the findings in the present study, benzoic acid may act on NQO1, AKR1C3, AKR1C1, GPX2, TXNRD1, SRXN1, and SLC7A11 and inhibit ferroptosis in the airway epithelium to alleviate COPD, but further studies on this are needed. Other novel therapies have also been developed, such as the use of Nrf2 activators, showing promise for treating COPD patients. Several Nrf2 activators have the potential to prevent damage caused by cigarette smoke. For example, following chronic CS exposure, CDDO-Im was found to induce more significant upregulation of Nrf2 and its target genes, attenuating CS-induced pulmonary oxidative stress, tissue destruction, and even pulmonary hypertension in wild-type mice; however, these protective effects were not significantly observed in Nrf2-deficient mice (61). Furthermore, 2 well-known Nrf2 activators, radicol and andrographolide, not only prevent CS/CSE-induced injury but also control infections that exacerbate COPD. In a recent study, radicol was reported to counteract CSE-induced oxidative damage by activating Nrf2 signaling in a rat alveolar epithelial cell line (62). To determine the role of dysregulation of the FRHGs in COPD, further validation of our results in an appropriate animal model is required. It should also not be overlooked how early it is important for people with COPD to quit smoking. The results of the present study further validate this idea, showing that the expression levels of FRHGs in former smokers can be restored to normal after quitting, and we have reason to believe that the prognosis of smokers with COPD who quit smoking will be better than that of those who continue to smoke.

It should also be noted that airway inflammation caused by cigarette smoke is also associated with immune infiltration in COPD patients, and how to construct the ceRNA regulatory network is also worth attention. Combining the construction of ceRNA network with the analysis of immune cells based on immune infiltration will help to identify diagnostic markers of COPD, thus contributing to the clinical management and treatment

of COPD, which requires more in-depth exploration and research.

The present study has several limitations. Firstly, because few studies on the role of ferroptosis in COPD have been performed, and only the FerDb database currently provides information on ferroptosis-related genes, more related genes remain to be discovered. Secondly, although all 7 screened FRHGs have been reported to mediate ferroptosis, there is no evidence that they can regulate ferroptosis in COPD. Therefore, further experimental evidence is needed to validate the ferroptosis regulatory function of these genes in COPD. However, although these animal models can morphologically reproduce some of the features of human COPD, there are currently no available animal models that reproduce the gene expression profile of COPD well, which leads to validation of potentially inaccurate and even contradictory findings, so we also look forward to the emergence of more ethical genetically humanized animal models. Thirdly, prospective clinical trial cohorts and more in-depth molecular biology experiments need to be designed and conducted to further validate the mechanism of action of these 7 ferroptosis-related genes in COPD development and progression.

Conclusions

In this study, we identified 7 potential ferroptosis hub genes (*NQO1*, *AKR1C3*, *AKR1C1*, *GPX2*, *TXNRD1*, *SRXN1*, *SLC7A11*) which exhibit good diagnostic properties and constructed a network of associated mRNA-miRNA pathways. Furthermore, based on these 7 ferroptosis hub genes, we found that benzoic acid showed high drug targeting relevance. The above findings deepen our understanding of the unique relationship between ferroptosis and COPD, and indicate that in-depth study of ferroptosis may provide therapeutic targets and biomarkers for COPD patients.

Acknowledgments

Funding: This work was supported by the Basic Research Program of Guangzhou (No. 202102010224), Clinical Transformation Program of the First Affiliated Hospital of Guangzhou Medical University (Nos. ZH201802 and ZH201914), Opening Project of State Key Laboratory of Respiratory Disease (No. SKLRD-0P-202115), the grant of State Key Laboratory of Respiratory Disease (No. SKLRD-Z-202203), the project of the department

of education Guangdong province, Natural Science Foundation of Guangdong Province (No. 2018A030310172) and 2021 Characteristic innovation projects of Colleges and universities in Guangdong Province (No. 2021KTSCX090).

Footnote

Reporting Checklist: The authors have completed the STREGA reporting checklist. Available at <https://atm.amegroupp.com/article/view/10.21037/atm-22-1009/rc>

Conflicts of Interest: All authors have completed the ICMJE uniform disclosure form (available at <https://atm.amegroupp.com/article/view/10.21037/atm-22-1009/coif>). The authors have no conflicts of interest to declare.

Ethical Statement: The authors are accountable for all aspects of the work in ensuring that questions related to the accuracy or integrity of any part of the work are appropriately investigated and resolved. The study was conducted in accordance with the Declaration of Helsinki (as revised in 2013).

Open Access Statement: This is an Open Access article distributed in accordance with the Creative Commons Attribution-NonCommercial-NoDerivs 4.0 International License (CC BY-NC-ND 4.0), which permits the non-commercial replication and distribution of the article with the strict proviso that no changes or edits are made and the original work is properly cited (including links to both the formal publication through the relevant DOI and the license). See: <https://creativecommons.org/licenses/by-nc-nd/4.0/>.

References

- Rabe KF, Watz H. Chronic obstructive pulmonary disease. *Lancet* 2017;389:1931-40.
- Silvestri GA, Young RP. Strange Bedfellows: The Interaction between COPD and Lung Cancer in the Context of Lung Cancer Screening. *Ann Am Thorac Soc* 2020;17:810-2.
- Yuan C, Chang, Lu G, et al. Genetic polymorphism and chronic obstructive pulmonary disease. *Int J Chron Obstruct Pulmon Dis* 2017;12:1385-93.
- Hikichi M, Mizumura K, Maruoka S, et al. Pathogenesis of chronic obstructive pulmonary disease (COPD) induced by cigarette smoke. *J Thorac Dis* 2019;11:S2129-40.
- Csoma B, Bikov A, Nagy L, et al. Dysregulation of the endothelial nitric oxide pathway is associated with airway inflammation in COPD. *Respir Res* 2019;20:156.
- Zheng M, Hong W, Gao M, et al. Long Noncoding RNA COPDA1 Promotes Airway Smooth Muscle Cell Proliferation in Chronic Obstructive Pulmonary Disease. *Am J Respir Cell Mol Biol* 2019;61:584-96.
- Zong D, Li J, Cai S, et al. Notch1 regulates endothelial apoptosis via the ERK pathway in chronic obstructive pulmonary disease. *Am J Physiol Cell Physiol* 2018;315:C330-40.
- Gouzi F, Blaquièrre M, Catteau M, et al. Oxidative stress regulates autophagy in cultured muscle cells of patients with chronic obstructive pulmonary disease. *J Cell Physiol* 2018;233:9629-39.
- Yoshida M, Minagawa S, Araya J, et al. Involvement of cigarette smoke-induced epithelial cell ferroptosis in COPD pathogenesis. *Nat Commun* 2019;10:3145.
- Dixon SJ, Lemberg KM, Lamprecht MR, et al. Ferroptosis: an iron-dependent form of nonapoptotic cell death. *Cell* 2012;149:1060-72.
- Stockwell BR, Friedmann Angeli JP, Bayir H, et al. Ferroptosis: A Regulated Cell Death Nexus Linking Metabolism, Redox Biology, and Disease. *Cell* 2017;171:273-85.
- Zhao J, Dar HH, Deng Y, et al. PEBP1 acts as a rheostat between prosurvival autophagy and ferroptotic death in asthmatic epithelial cells. *Proc Natl Acad Sci U S A* 2020;117:14376-85.
- Xu Y, Li X, Cheng Y, et al. Inhibition of ACSL4 attenuates ferroptotic damage after pulmonary ischemia-reperfusion. *FASEB J* 2020;34:16262-75.
- Minagawa S, Yoshida M, Araya J, et al. Regulated Necrosis in Pulmonary Disease. A Focus on Necroptosis and Ferroptosis. *Am J Respir Cell Mol Biol* 2020;62:554-62.
- Rab A, Rowe SM, Raju SV, et al. Cigarette smoke and CFTR: implications in the pathogenesis of COPD. *Am J Physiol Lung Cell Mol Physiol* 2013;305:L530-41.
- Gould NS, Min E, Gauthier S, et al. Lung glutathione adaptive responses to cigarette smoke exposure. *Respir Res* 2011;12:133.
- Hogg JC, Macklem PT, Thurlbeck WM. Site and nature of airway obstruction in chronic obstructive lung disease. *N Engl J Med* 1968;278:1355-60.
- Van Brabant H, Cauberghe M, Verbeken E, et al. Partitioning of pulmonary impedance in excised human and canine lungs. *J Appl Physiol Respir Environ Exerc Physiol* 1983;55:1733-42.
- Yanai M, Sekizawa K, Ohru T, et al. Site of airway

- obstruction in pulmonary disease: direct measurement of intrabronchial pressure. *J Appl Physiol* (1985) 1992;72:1016-23.
20. Zhu M, Ye M, Wang J, et al. Construction of Potential miRNA-mRNA Regulatory Network in COPD Plasma by Bioinformatics Analysis. *Int J Chron Obstruct Pulmon Dis* 2020;15:2135-45.
 21. Regan EA, Hersh CP, Castaldi PJ, et al. Omics and the Search for Blood Biomarkers in Chronic Obstructive Pulmonary Disease. Insights from COPDGene. *Am J Respir Cell Mol Biol* 2019;61:143-9.
 22. Davis S, Meltzer PS. GEOquery: a bridge between the Gene Expression Omnibus (GEO) and BioConductor. *Bioinformatics* 2007;23:1846-7.
 23. Gu Z, Eils R, Schlesner M. Complex heatmaps reveal patterns and correlations in multidimensional genomic data. *Bioinformatics* 2016;32:2847-9.
 24. Wu Y, Guan S, Ge Y, et al. Cigarette smoke promotes chronic obstructive pulmonary disease (COPD) through the miR-130a/Wnt1 axis. *Toxicol In Vitro* 2020;65:104770.
 25. Xu H, Ling M, Xue J, et al. Exosomal microRNA-21 derived from bronchial epithelial cells is involved in aberrant epithelium-fibroblast cross-talk in COPD induced by cigarette smoking. *Theranostics* 2018;8:5419-33.
 26. Roffel MP, Maes T, Brandsma CA, et al. MiR-223 is increased in lungs of patients with COPD and modulates cigarette smoke-induced pulmonary inflammation. *Am J Physiol Lung Cell Mol Physiol* 2021;321:L1091-104.
 27. Zeng Q, Zeng J. Inhibition of miR-494-3p alleviates oxidative stress-induced cell senescence and inflammation in the primary epithelial cells of COPD patients. *Int Immunopharmacol* 2021;92:107044.
 28. Osei ET, Florez-Sampedro L, Tasena H, et al. miR-146a-5p plays an essential role in the aberrant epithelial-fibroblast cross-talk in COPD. *Eur Respir J* 2017;49:1602538.
 29. Shen Y, Lu H, Song G. MiR-221-3p and miR-92a-3p enhances smoking-induced inflammation in COPD. *J Clin Lab Anal* 2021;35:e23857.
 30. Shen Z, Tang W, Guo J, et al. miR-483-5p plays a protective role in chronic obstructive pulmonary disease. *Int J Mol Med* 2017;40:193-200.
 31. Conickx G, Mestdagh P, Avila Cobos F, et al. MicroRNA Profiling Reveals a Role for MicroRNA-218-5p in the Pathogenesis of Chronic Obstructive Pulmonary Disease. *Am J Respir Crit Care Med* 2017;195:43-56.
 32. Nouws J, Wan F, Finnemore E, et al. MicroRNA miR-24-3p reduces DNA damage responses, apoptosis, and susceptibility to chronic obstructive pulmonary disease. *JCI Insight* 2021;6:134218.
 33. Song B, Ye L, Wu S, et al. Long non-coding RNA MEG3 regulates CSE-induced apoptosis and inflammation via regulating miR-218 in 16HBE cells. *Biochem Biophys Res Commun* 2020;521:368-74.
 34. Gu W, Yuan Y, Yang H, et al. Role of miR-195 in cigarette smoke-induced chronic obstructive pulmonary disease. *Int Immunopharmacol* 2018;55:49-54.
 35. Du Y, Ding Y, Chen X, et al. MicroRNA-181c inhibits cigarette smoke-induced chronic obstructive pulmonary disease by regulating CCN1 expression. *Respir Res* 2017;18:155.
 36. Kaur G, Begum R, Thota S, et al. A systematic review of smoking-related epigenetic alterations. *Arch Toxicol* 2019;93:2715-40.
 37. Zhao N, Yu MJ, Xu J, et al. microRNA-29b mediates Th17/Treg imbalance in chronic obstructive pulmonary disease by targeting IL-22. *J Biol Regul Homeost Agents* 2021;35:987-99.
 38. Chen P, Jiang P, Chen J, et al. XIST promotes apoptosis and the inflammatory response in CSE-stimulated cells via the miR-200c-3p/EGR3 axis. *BMC Pulm Med* 2021;21:215.
 39. Shen HF, Liu Y, Qu PP, et al. MiR-361-5p/abca1 and MiR-196-5p/arhgef12 Axis Involved in γ -Sitosterol Inducing Dual Anti-Proliferative Effects on Bronchial Epithelial Cells of Chronic Obstructive Pulmonary Disease. *Int J Chron Obstruct Pulmon Dis* 2021;16:2741-53.
 40. Liu L, Wan C, Zhang W, et al. MiR-146a regulates PM1-induced inflammation via NF- κ B signaling pathway in BEAS-2B cells. *Environ Toxicol* 2018;33:743-51.
 41. Deeks ED, Dhillon S. Strontium ranelate: a review of its use in the treatment of postmenopausal osteoporosis. *Drugs* 2010;70:733-59.
 42. Sakai H, Horiguchi M, Akita T, et al. Effect of 4-(5,6,7,8-Tetrahydro-5,5,8,8-Tetramethyl-2-Naphthalenyl)CarbamoylBenzoic Acid (Am80) on Alveolar Regeneration in Adiponectin Deficient-Mice Showing a Chronic Obstructive Pulmonary Disease-Like Pathophysiology. *J Pharmacol Exp Ther* 2017;361:501-5.
 43. Zhou N, Bao J. FerrDb: a manually curated resource for regulators and markers of ferroptosis and ferroptosis-disease associations. *Database (Oxford)* 2020;2020:baaa021.
 44. Singh A, Rangasamy T, Thimmulappa RK, et al.

- Glutathione peroxidase 2, the major cigarette smoke-inducible isoform of GPX in lungs, is regulated by Nrf2. *Am J Respir Cell Mol Biol* 2006;35:639-50.
45. Tian Q, Zhou Y, Zhu L, et al. Development and Validation of a Ferroptosis-Related Gene Signature for Overall Survival Prediction in Lung Adenocarcinoma. *Front Cell Dev Biol* 2021;9:684259.
 46. Koppula P, Zhuang L, Gan B. Cystine transporter SLC7A11/xCT in cancer: ferroptosis, nutrient dependency, and cancer therapy. *Protein Cell* 2021;12:599-620.
 47. Zhu K, Li Y, Deng C, et al. Significant association of PKM2 and NQO1 proteins with poor prognosis in breast cancer. *Pathol Res Pract* 2020;216:153173.
 48. Burczynski ME, Sridhar GR, Palackal NT, et al. The reactive oxygen species--and Michael acceptor-inducible human aldo-keto reductase AKR1C1 reduces the alpha,beta-unsaturated aldehyde 4-hydroxy-2-nonenal to 1,4-dihydroxy-2-nonene. *J Biol Chem* 2001;276:2890-7.
 49. Li L, Lin G, Gu H, et al. Effects of Srxn1 on growth and Notch signalling of astrocyte induced by hydrogen peroxide. *Artif Cells Nanomed Biotechnol* 2019;47:1917-23.
 50. Dai B, Yoo SY, Bartholomeusz G, et al. KEAP1-dependent synthetic lethality induced by AKT and TXNRD1 inhibitors in lung cancer. *Cancer Res* 2013;73:5532-43.
 51. Dinkova-Kostova AT, Kostov RV, Kazantsev AG. The role of Nrf2 signaling in counteracting neurodegenerative diseases. *FEBS J* 2018;285:3576-90.
 52. Fan Z, Wirth AK, Chen D, et al. Nrf2-Keap1 pathway promotes cell proliferation and diminishes ferroptosis. *Oncogenesis* 2017;6:e371.
 53. La Rosa P, Bertini ES, Piemonte F. The NRF2 Signaling Network Defines Clinical Biomarkers and Therapeutic Opportunity in Friedreich's Ataxia. *Int J Mol Sci* 2020;21:916.
 54. Dodson M, Castro-Portuguez R, Zhang DD. NRF2 plays a critical role in mitigating lipid peroxidation and ferroptosis. *Redox Biol* 2019;23:101107.
 55. Gagliardi M, Cotella D, Santoro C, et al. Aldo-keto reductases protect metastatic melanoma from ER stress-independent ferroptosis. *Cell Death Dis* 2019;10:902.
 56. Hua CC, Chang LC, Tseng JC, et al. Functional haplotypes in the promoter region of transcription factor Nrf2 in chronic obstructive pulmonary disease. *Dis Markers* 2010;28:185-93.
 57. Rangasamy T, Cho CY, Thimmulappa RK, et al. Genetic ablation of Nrf2 enhances susceptibility to cigarette smoke-induced emphysema in mice. *J Clin Invest* 2004;114:1248-59.
 58. Croasdell Lucchini A, Gachanja NN, Rossi AG, et al. Epithelial Cells and Inflammation in Pulmonary Wound Repair. *Cells* 2021;10:339.
 59. Massaro GD, Massaro D. Retinoic acid treatment abrogates elastase-induced pulmonary emphysema in rats. *Nat Med* 1997;3:675-7.
 60. Nakanishi K, Takeda Y, Tetsumoto S, et al. Involvement of endothelial apoptosis underlying chronic obstructive pulmonary disease-like phenotype in adiponectin-null mice: implications for therapy. *Am J Respir Crit Care Med* 2011;183:1164-75.
 61. Sussan TE, Rangasamy T, Blake DJ, et al. Targeting Nrf2 with the triterpenoid CDDO-imidazole attenuates cigarette smoke-induced emphysema and cardiac dysfunction in mice. *Proc Natl Acad Sci U S A* 2009;106:250-5.
 62. Jiao Z, Chang J, Li J, et al. Sulforaphane increases Nrf2 expression and protects alveolar epithelial cells against injury caused by cigarette smoke extract. *Mol Med Rep* 2017;16:1241-7.

(English Language Editor: C. Betlazar-Maseh)

Cite this article as: Lin Z, Xu Y, Guan L, Qin L, Ding J, Zhang Q, Zhou L. Seven ferroptosis-specific expressed genes are considered as potential biomarkers for the diagnosis and treatment of cigarette smoke-induced chronic obstructive pulmonary disease. *Ann Transl Med* 2022;10(6):331. doi: 10.21037/atm-22-1009

Table S1 Commonly differentially expressed among GSE10006, GSE11784 AND GSE20257

Gene.Symbol	Up/Down
<i>CYP1B1</i>	Upregulated
<i>CYP1A1</i>	Upregulated
<i>AKR1B10</i>	Upregulated
<i>UCHL1</i>	Upregulated
<i>GAD1</i>	Upregulated
<i>CEACAM5</i>	Upregulated
<i>SPP1</i>	Upregulated
<i>MUCL1</i>	Upregulated
<i>GPX2</i>	Upregulated
<i>LOC284825</i>	Upregulated
<i>SPRR3</i>	Upregulated
<i>TPRXL</i>	Upregulated
<i>CCL2</i>	Upregulated
<i>SLC7A11</i>	Upregulated
<i>CXCL14</i>	Upregulated
<i>ALDH3A1</i>	Upregulated
<i>CABYR</i>	Upregulated
<i>SFRP2</i>	Upregulated
<i>ST3GAL4-AS1</i>	Upregulated
<i>ADH7</i>	Upregulated
<i>HOTS</i>	Upregulated
<i>TCN1</i>	Upregulated
<i>CLEC5A</i>	Upregulated
<i>B3GNT6</i>	Upregulated
<i>JAKMIP3</i>	Upregulated
<i>MUC12</i>	Upregulated
<i>DTNA</i>	Upregulated
<i>KRT6A</i>	Upregulated
<i>MEP1A</i>	Upregulated
<i>AHRR</i>	Upregulated
<i>BPIFB2</i>	Upregulated
<i>HS3ST3A1</i>	Upregulated
<i>SRPX2</i>	Upregulated
<i>ELFN2</i>	Upregulated
<i>LOC344887</i>	Upregulated
<i>LOC102724094</i>	Upregulated
<i>ME1</i>	Upregulated
<i>SCG3</i>	Upregulated

Table S1 (continued)**Table S1** (continued)

Gene.Symbol	Up/Down
<i>PHEX</i>	Upregulated
<i>CBR1</i>	Upregulated
<i>STATH</i>	Upregulated
<i>SPRR1B</i>	Upregulated
<i>CYP4F11</i>	Upregulated
<i>PTPRH</i>	Upregulated
<i>EGF</i>	Upregulated
<i>DUOX2</i>	Upregulated
<i>MUC5AC</i>	Upregulated
<i>SCEL</i>	Upregulated
<i>HOXA1</i>	Upregulated
<i>NR0B1</i>	Upregulated
<i>LRRC31</i>	Upregulated
<i>AKR1C3</i>	Upregulated
<i>CNGB1</i>	Upregulated
<i>CYP4F2</i>	Upregulated
<i>RP11-619L19.1</i>	Upregulated
<i>BMP4</i>	Upregulated
<i>MMP12</i>	Upregulated
<i>RP11-203B7.1</i>	Upregulated
<i>ENAM</i>	Upregulated
<i>CYP4F3</i>	Upregulated
<i>TREM2</i>	Upregulated
<i>CLDN10</i>	Upregulated
<i>NQO1</i>	Upregulated
<i>CTCFL</i>	Upregulated
<i>FCGR2B</i>	Upregulated
<i>DEFB1</i>	Upregulated
<i>UPK1B</i>	Upregulated
<i>RP11-524D16__A.3</i>	Upregulated
<i>PIR</i>	Upregulated
<i>PHLDA1</i>	Upregulated
<i>CBR3</i>	Upregulated
<i>BPIFA2</i>	Upregulated
<i>AKR1C1</i>	Upregulated
<i>C22orf42</i>	Upregulated
<i>ADM</i>	Upregulated
<i>SRXN1</i>	Upregulated
<i>mir-223</i>	Upregulated
<i>IL19</i>	Upregulated

Table S1 (continued)

Table S1 (continued)

Gene.Symbol	Up/Down
<i>DNAJC12</i>	Upregulated
<i>SIX3</i>	Upregulated
<i>PANX3</i>	Upregulated
<i>CALCA</i>	Upregulated
<i>RP13-238F13.5</i>	Upregulated
<i>KRT40</i>	Upregulated
<i>CDH2</i>	Upregulated
<i>CLIP4</i>	Upregulated
<i>CCL7</i>	Upregulated
<i>PLA2G7</i>	Upregulated
<i>ASCL3</i>	Upregulated
<i>REG3G</i>	Upregulated
<i>OSGIN1</i>	Upregulated
<i>HTR2B</i>	Upregulated
<i>FAM3B</i>	Upregulated
<i>SIGLEC11</i>	Upregulated
<i>TXNRD1</i>	Upregulated
<i>TMPRSS11E</i>	Upregulated
<i>SAMD5</i>	Upregulated
<i>PRSS50</i>	Upregulated
<i>BCL2A1</i>	Upregulated
<i>ATP6V0A4</i>	Upregulated
<i>CEMIP</i>	Upregulated
<i>LHX6</i>	Upregulated
<i>AGPAT9</i>	Upregulated
<i>BAALC</i>	Upregulated
<i>GFRA3</i>	Upregulated
<i>LOXHD1</i>	Upregulated
<i>PLAT</i>	Upregulated
<i>RP11-96H17.1</i>	Upregulated
<i>LINC00403</i>	Upregulated
<i>AKR1B1</i>	Upregulated
<i>ITGAX</i>	Upregulated
<i>FCN1</i>	Upregulated
<i>MCEMP1</i>	Upregulated
<i>OSTM1-AS1</i>	Upregulated
<i>C2orf70</i>	Upregulated
<i>HGD</i>	Upregulated
<i>TMCC3</i>	Upregulated
<i>ATXN8OS</i>	Upregulated

Table S1 (continued)

Table S1 (continued)

Gene.Symbol	Up/Down
<i>MRC1</i>	Upregulated
<i>PSG7</i>	Upregulated
<i>LOC101929591</i>	Upregulated
<i>DUSP5P1</i>	Upregulated
<i>HTATIP2</i>	Upregulated
<i>CLMP</i>	Upregulated
<i>MMP19</i>	Upregulated
<i>FOXD3-AS1</i>	Upregulated
<i>TKT</i>	Upregulated
<i>RNFT2</i>	Upregulated
<i>WDR72</i>	Upregulated
<i>SPINK5</i>	Upregulated
<i>NAV1</i>	Upregulated
<i>AZGP1</i>	Upregulated
<i>FAM20C</i>	Upregulated
<i>ADRB3</i>	Upregulated
<i>MTHFD2</i>	Upregulated
<i>CHST1</i>	Upregulated
<i>RP11-400N13.1</i>	Upregulated
<i>OR8D2</i>	Upregulated
<i>CD163L1</i>	Upregulated
<i>CD109</i>	Upregulated
<i>SMOC1</i>	Upregulated
<i>EPHB1</i>	Upregulated
<i>CPE</i>	Upregulated
<i>ATP8B5P</i>	Upregulated
<i>CACNA2D3</i>	Upregulated
<i>PTPRG-AS1</i>	Upregulated
<i>SLC2A3</i>	Upregulated
<i>LOC101927690</i>	Upregulated
<i>LOC285423</i>	Upregulated
<i>MLKL</i>	Upregulated
<i>LYPD3</i>	Upregulated
<i>CTHRC1</i>	Upregulated
<i>TUBB2B</i>	Upregulated
<i>ITLN1</i>	Downregulated
<i>NAV3</i>	Downregulated
<i>TACR1</i>	Downregulated
<i>LTF</i>	Downregulated
<i>MT1M</i>	Downregulated

Table S1 (continued)

Table S1 (continued)

Gene.Symbol	Up/Down
SEC14L3	Downregulated
C3	Downregulated
TFPI2	Downregulated
HSD17B2	Downregulated
LOC100130744	Downregulated
PPP1R16B	Downregulated
KCNA1	Downregulated
TMEM45A	Downregulated
CX3CL1	Downregulated
CDKAL1	Downregulated
MAOB	Downregulated
NT5E	Downregulated
ZSCAN4	Downregulated
FAM65C	Downregulated
LOC338667	Downregulated
LOC100505874	Downregulated
AFAP1L1	Downregulated
NPAS3	Downregulated
WNK4	Downregulated
CNN3	Downregulated
SHISA9	Downregulated
RTN4RL1	Downregulated
AVPR1A	Downregulated
LOC283177	Downregulated
C8orf12	Downregulated
PLK2	Downregulated
ITM2A	Downregulated
MUC5B	Downregulated
SLIT2	Downregulated
FHOD3	Downregulated
FOXA2	Downregulated
SERPINB10	Downregulated
LOC100507560	Downregulated
PNMA2	Downregulated
C1QTNF4	Downregulated
CES1P1	Downregulated
ANO4	Downregulated
CCL20	Downregulated
SLC29A1	Downregulated
PCSK6	Downregulated

Table S1 (continued)**Table S1** (continued)

Gene.Symbol	Up/Down
PWAR5	Downregulated
THSD7A	Downregulated
TMEM178A	Downregulated
PROS1	Downregulated
GRM5	Downregulated
RP11-355F16.1	Downregulated
TPM2	Downregulated
SMIM1	Downregulated
CSGALNACT1	Downregulated
CYP4X1	Downregulated
PANK1	Downregulated
PCDH17	Downregulated
PYGO1	Downregulated
PRKAR2B	Downregulated
LAG3	Downregulated
ITGB2-AS1	Downregulated
PAX1	Downregulated
ZBTB16	Downregulated
VGLL3	Downregulated
SGCE	Downregulated
MGP	Downregulated
MMP7	Downregulated

Table S2 Ferroptosis genes

FERROPTOSIS GENES
SLC7A11
GPX4
AKR1C1
AKR1C2
AKR1C3
RB1
HSPB1
HSF1
NFE2L2
SQSTM1
NQO1
HMOX1
FTH1
MUC1
MT1G
SLC40A1
CISD1
HSPA5
ATF4
TP53
HELLS
SCD
FADS2
SRC
STAT3
PML
NFS1
TP63
CDKN1A
MIR137
VDAC2
FH
CISD2
MIR9-1
MIR9-2

Table S2 (continued)

Table S2 (continued)

FERROPTOSIS GENES
MIR9-3
CBS
ISCU
ACSL3
OTUB1
CD44
LINC00336
BRD4
PRDX6
MIR17
SESN2
NF2
ARNTL
HIF1A
JUN
CA9
TMBIM4
PLIN2
AIFM2
LAMP2
ZFP36
PROM2
CHMP5
CHMP6
CAV1
GCH1
PTGS2
DUSP1
NOS2
NCF2
MT3
UBC
ALB
TXNRD1
SRXN1

Table S2 (continued)

Table S2 (continued)

FERROPTOSIS GENES
GPX2
BNIP3
OXSRI
SELENOS
ANGPTL7
CHAC1
DDIT4
LOC284561
ASNS
TSC22D3
DDIT3
JDP2
SLC1A4
PCK2
TXNIP
VLDLR
GPT2
PSAT1
LURAP1L
SLC7A5
HERPUD1
XBP1
ATF3
SLC3A2
ZNF419
KLHL24
TRIB3
ZFP69B
ATP6V1G2
VEGFA
GDF15
TUBE1
ARRDC3
CEBPG
SNORA16A

Table S2 (continued)

Table S2 (continued)

FERROPTOSIS GENES
RGS4
BLOC1S5-TXNDC5
LOC390705
EIF2S1
HSD17B11
AGPAT3
SETD1B
TF
FTL
RPL8
ATP5MC3
TFRC
MAFG
DRD5
DRD4
MAP3K5
MAPK14
SLC2A1
SLC2A3
SLC2A6
SLC2A8
SLC2A12
GLUT13
SLC2A14
EIF2AK4
ALOX5
ALOX12
ALOX15
HMGB1
ELAVL1
HBA1
NNMT
PLIN4
HIC1
STMN1

Table S2 (continued)

Table S2 (*continued*)

FERROPTOSIS GENES
<i>RRM2</i>
<i>CAPG</i>
<i>HNF4A</i>
<i>NGB</i>
<i>YWHAE</i>
<i>GABPB1</i>
<i>AURKA</i>
<i>MIR4715</i>
<i>RIPK1</i>
<i>PRDX1</i>
<i>MIR30B</i>
<i>IREB2</i>
<i>CS</i>
<i>EMC2</i>
<i>ACSF2</i>
<i>NOX1</i>
<i>CYBB</i>
<i>NOX3</i>
<i>NOX4</i>
<i>NOX5</i>
<i>DUOX1</i>
<i>DUOX2</i>
<i>G6PD</i>
<i>PGD</i>
<i>ACSL4</i>
<i>LPCAT3</i>
<i>NRAS</i>
<i>KRAS</i>
<i>HRAS</i>
<i>CARS1</i>
<i>KEAP1</i>
<i>ATG5</i>
<i>ATG7</i>
<i>NCOA4</i>
<i>ALOX12B</i>

Table S2 (*continued*)**Table S2** (*continued*)

FERROPTOSIS GENES
<i>ALOX15B</i>
<i>ALOXE3</i>
<i>PHKG2</i>
<i>SAT1</i>
<i>EGFR</i>
<i>MAPK3</i>
<i>MAPK1</i>
<i>ZEB1</i>
<i>DPP4</i>
<i>CDKN2A</i>
<i>PEBP1</i>
<i>SOCS1</i>
<i>CDO1</i>
<i>MYB</i>
<i>SLC1A5</i>
<i>LINC00472</i>
<i>GOT1</i>
<i>BECN1</i>
<i>PRKAA2</i>
<i>PRKAA1</i>
<i>BAP1</i>
<i>ABCC1</i>
<i>MIR6852</i>
<i>ACVR1B</i>
<i>TGFBR1</i>
<i>IFNG</i>
<i>ANO6</i>
<i>TNFAIP3</i>
<i>ATM</i>
<i>YY1AP1</i>
<i>EGLN2</i>
<i>MIOX</i>
<i>TAZ</i>
<i>MTDH</i>
<i>IDH1</i>

Table S2 (*continued*)**Table S2** (*continued*)

FERROPTOSIS GENES
<i>FBXW7</i>
<i>PANX1</i>
<i>DNAJB6</i>
<i>LONP1</i>

Table S3 mRNA-miRNA pairs

ID	Target	TargetID
hsa-let-7e-5p	TXNRD1	7296
hsa-mir-26b-5p	TXNRD1	7296
hsa-mir-34a-5p	TXNRD1	7296
hsa-mir-186-5p	TXNRD1	7296
hsa-mir-155-5p	TXNRD1	7296
hsa-mir-409-3p	TXNRD1	7296
hsa-mir-504-5p	TXNRD1	7296
hsa-mir-505-3p	TXNRD1	7296
hsa-mir-421	TXNRD1	7296
hsa-mir-124-5p	TXNRD1	7296
hsa-mir-1323	TXNRD1	7296
hsa-mir-1298-5p	TXNRD1	7296
hsa-mir-1206	TXNRD1	7296
hsa-mir-1257	TXNRD1	7296
hsa-mir-548o-3p	TXNRD1	7296
hsa-mir-4272	TXNRD1	7296
hsa-mir-3611	TXNRD1	7296
hsa-mir-219b-5p	TXNRD1	7296
hsa-mir-4672	TXNRD1	7296
hsa-mir-4709-5p	TXNRD1	7296
hsa-mir-4714-3p	TXNRD1	7296
hsa-mir-5587-5p	TXNRD1	7296
hsa-mir-6768-5p	TXNRD1	7296
hsa-mir-6853-3p	TXNRD1	7296
hsa-mir-7159-5p	TXNRD1	7296
hsa-mir-1243	TXNRD1	7296
hsa-mir-124-3p	TXNRD1	7296
hsa-mir-125a-5p	TXNRD1	7296
hsa-mir-125b-5p	TXNRD1	7296
hsa-mir-130b-5p	TXNRD1	7296
hsa-mir-141-3p	TXNRD1	7296
hsa-mir-148a-3p	TXNRD1	7296
hsa-mir-148b-3p	TXNRD1	7296
hsa-mir-149-5p	TXNRD1	7296
hsa-mir-15b-3p	TXNRD1	7296
hsa-mir-16-5p	TXNRD1	7296
hsa-mir-181a-2-3p	TXNRD1	7296
hsa-mir-1825	TXNRD1	7296
hsa-mir-182-5p	TXNRD1	7296

Table S3 (continued)**Table S3** (continued)

ID	Target	TargetID
hsa-mir-191-5p	TXNRD1	7296
hsa-mir-193a-3p	TXNRD1	7296
hsa-mir-193b-3p	TXNRD1	7296
hsa-mir-196a-5p	TXNRD1	7296
hsa-mir-203a-3p	TXNRD1	7296
hsa-mir-21-3p	TXNRD1	7296
hsa-mir-224-5p	TXNRD1	7296
hsa-mir-22-5p	TXNRD1	7296
hsa-mir-23a-3p	TXNRD1	7296
hsa-mir-23b-3p	TXNRD1	7296
hsa-mir-24-1-5p	TXNRD1	7296
hsa-mir-24-2-5p	TXNRD1	7296
hsa-mir-24-3p	TXNRD1	7296
hsa-mir-25-3p	TXNRD1	7296
hsa-mir-26a-5p	TXNRD1	7296
hsa-mir-27a-5p	TXNRD1	7296
hsa-mir-29a-3p	TXNRD1	7296
hsa-mir-29b-3p	TXNRD1	7296
hsa-mir-29c-3p	TXNRD1	7296
hsa-mir-330-3p	TXNRD1	7296
hsa-mir-331-5p	TXNRD1	7296
hsa-mir-338-3p	TXNRD1	7296
hsa-mir-339-3p	TXNRD1	7296
hsa-mir-374c-5p	TXNRD1	7296
hsa-mir-376c-3p	TXNRD1	7296
hsa-mir-425-5p	TXNRD1	7296
hsa-mir-4422	TXNRD1	7296
hsa-mir-455-3p	TXNRD1	7296
hsa-mir-4766-3p	TXNRD1	7296
hsa-mir-500a-3p	TXNRD1	7296
hsa-mir-502-3p	TXNRD1	7296
hsa-mir-505-5p	TXNRD1	7296
hsa-mir-518a-5p	TXNRD1	7296
hsa-mir-522-5p	TXNRD1	7296
hsa-mir-527	TXNRD1	7296
hsa-mir-545-3p	TXNRD1	7296
hsa-mir-548n	TXNRD1	7296
hsa-mir-551b-5p	TXNRD1	7296
hsa-mir-575	TXNRD1	7296

Table S3 (continued)

Table S3 (continued)

ID	Target	TargetID
hsa-mir-587	TXNRD1	7296
hsa-mir-590-3p	TXNRD1	7296
hsa-mir-624-3p	TXNRD1	7296
hsa-mir-634	TXNRD1	7296
hsa-mir-7-1-3p	TXNRD1	7296
hsa-mir-7-2-3p	TXNRD1	7296
hsa-mir-935	TXNRD1	7296
hsa-mir-942-5p	TXNRD1	7296
hsa-mir-1-3p	TXNRD1	7296
hsa-mir-138-5p	TXNRD1	7296
hsa-mir-200b-3p	TXNRD1	7296
hsa-mir-423-5p	TXNRD1	7296
hsa-mir-374a-5p	TXNRD1	7296
hsa-mir-96-5p	SRXN1	140809
hsa-mir-1-3p	SRXN1	140809
hsa-mir-200a-5p	SRXN1	140809
hsa-mir-505-3p	SRXN1	140809
hsa-mir-600	SRXN1	140809
hsa-mir-200b-5p	SRXN1	140809
hsa-mir-150-3p	SRXN1	140809
hsa-mir-499a-3p	SRXN1	140809
hsa-mir-3974	SRXN1	140809
hsa-mir-499b-3p	SRXN1	140809
hsa-mir-5579-5p	SRXN1	140809
hsa-mir-6814-5p	SRXN1	140809
hsa-mir-6849-3p	SRXN1	140809
hsa-mir-7153-3p	SRXN1	140809
hsa-mir-103a-3p	SRXN1	140809
hsa-mir-155-5p	SRXN1	140809
hsa-mir-191-5p	SRXN1	140809
hsa-mir-10b-5p	SRXN1	140809
hsa-mir-124-3p	SRXN1	140809
hsa-mir-146a-5p	SRXN1	140809
hsa-mir-195-5p	SRXN1	140809
hsa-mir-34a-5p	SRXN1	140809
hsa-mir-7-5p	SRXN1	140809
hsa-mir-374a-5p	SRXN1	140809
hsa-mir-1	SRXN1	140809
hsa-mir-17-5p	SLC7A11	23657
hsa-mir-19a-3p	SLC7A11	23657

Table S3 (continued)

Table S3 (continued)

ID	Target	TargetID
hsa-mir-19b-3p	SLC7A11	23657
hsa-mir-20a-5p	SLC7A11	23657
hsa-mir-25-3p	SLC7A11	23657
hsa-mir-26b-5p	SLC7A11	23657
hsa-mir-27a-3p	SLC7A11	23657
hsa-mir-30a-5p	SLC7A11	23657
hsa-mir-32-5p	SLC7A11	23657
hsa-mir-92a-3p	SLC7A11	23657
hsa-mir-93-5p	SLC7A11	23657
hsa-mir-106a-5p	SLC7A11	23657
hsa-mir-192-5p	SLC7A11	23657
hsa-mir-181a-5p	SLC7A11	23657
hsa-mir-215-5p	SLC7A11	23657
hsa-mir-218-5p	SLC7A11	23657
hsa-mir-122-5p	SLC7A11	23657
hsa-mir-128-3p	SLC7A11	23657
hsa-mir-142-3p	SLC7A11	23657
hsa-mir-150-5p	SLC7A11	23657
hsa-mir-155-5p	SLC7A11	23657
hsa-mir-106b-5p	SLC7A11	23657
hsa-mir-302a-3p	SLC7A11	23657
hsa-mir-363-3p	SLC7A11	23657
hsa-mir-302b-3p	SLC7A11	23657
hsa-mir-302c-3p	SLC7A11	23657
hsa-mir-302d-3p	SLC7A11	23657
hsa-mir-367-3p	SLC7A11	23657
hsa-mir-372-3p	SLC7A11	23657
hsa-mir-373-3p	SLC7A11	23657
hsa-mir-148b-3p	SLC7A11	23657
hsa-mir-20b-5p	SLC7A11	23657
hsa-mir-329-3p	SLC7A11	23657
hsa-mir-410-3p	SLC7A11	23657
hsa-mir-489-3p	SLC7A11	23657
hsa-mir-512-3p	SLC7A11	23657
hsa-mir-498	SLC7A11	23657
hsa-mir-520e	SLC7A11	23657
hsa-mir-520a-3p	SLC7A11	23657
hsa-mir-526b-3p	SLC7A11	23657
hsa-mir-520b	SLC7A11	23657
hsa-mir-520c-3p	SLC7A11	23657

Table S3 (continued)

Table S3 (continued)

ID	Target	TargetID
hsa-mir-519d-3p	SLC7A11	23657
hsa-mir-520d-3p	SLC7A11	23657
hsa-mir-520g-3p	SLC7A11	23657
hsa-mir-520h	SLC7A11	23657
hsa-mir-500a-3p	SLC7A11	23657
hsa-mir-92b-3p	SLC7A11	23657
hsa-mir-587	SLC7A11	23657
hsa-mir-595	SLC7A11	23657
hsa-mir-603	SLC7A11	23657
hsa-mir-767-5p	SLC7A11	23657
hsa-mir-223-5p	SLC7A11	23657
hsa-mir-186-3p	SLC7A11	23657
hsa-mir-362-3p	SLC7A11	23657
hsa-mir-340-5p	SLC7A11	23657
hsa-mir-505-5p	SLC7A11	23657
hsa-mir-574-5p	SLC7A11	23657
hsa-mir-302e	SLC7A11	23657
hsa-mir-1279	SLC7A11	23657
hsa-mir-1281	SLC7A11	23657
hsa-mir-1976	SLC7A11	23657
hsa-mir-548t-5p	SLC7A11	23657
hsa-mir-3163	SLC7A11	23657
hsa-mir-4279	SLC7A11	23657
hsa-mir-4282	SLC7A11	23657
hsa-mir-3941	SLC7A11	23657
hsa-mir-4532	SLC7A11	23657
hsa-mir-3913-3p	SLC7A11	23657
hsa-mir-4640-3p	SLC7A11	23657
hsa-mir-4722-3p	SLC7A11	23657
hsa-mir-4731-5p	SLC7A11	23657
hsa-mir-4789-5p	SLC7A11	23657
hsa-mir-4789-3p	SLC7A11	23657
hsa-mir-5011-5p	SLC7A11	23657
hsa-mir-5089-5p	SLC7A11	23657
hsa-mir-5193	SLC7A11	23657
hsa-mir-5571-5p	SLC7A11	23657
hsa-mir-5589-5p	SLC7A11	23657
hsa-mir-5589-3p	SLC7A11	23657
hsa-mir-5683	SLC7A11	23657
hsa-mir-1247-3p	SLC7A11	23657

Table S3 (continued)**Table S3** (continued)

ID	Target	TargetID
hsa-mir-1277-5p	SLC7A11	23657
hsa-mir-548az-5p	SLC7A11	23657
hsa-mir-6504-3p	SLC7A11	23657
hsa-mir-6506-5p	SLC7A11	23657
hsa-mir-190a-3p	SLC7A11	23657
hsa-mir-619-5p	SLC7A11	23657
hsa-mir-548e-5p	SLC7A11	23657
hsa-mir-6727-3p	SLC7A11	23657
hsa-mir-6747-3p	SLC7A11	23657
hsa-mir-6778-3p	SLC7A11	23657
hsa-mir-6791-3p	SLC7A11	23657
hsa-mir-6826-5p	SLC7A11	23657
hsa-mir-6829-3p	SLC7A11	23657
hsa-mir-6835-3p	SLC7A11	23657
hsa-mir-6867-5p	SLC7A11	23657
hsa-mir-6874-5p	SLC7A11	23657
hsa-mir-1-5p	SLC7A11	23657
hsa-mir-3653-5p	SLC7A11	23657
hsa-mir-8485	SLC7A11	23657
hsa-let-7g-3p	SLC7A11	23657
hsa-mir-100-5p	SLC7A11	23657
hsa-mir-130a-3p	SLC7A11	23657
hsa-mir-130b-3p	SLC7A11	23657
hsa-mir-138-2-3p	SLC7A11	23657
hsa-mir-148a-5p	SLC7A11	23657
hsa-mir-17-3p	SLC7A11	23657
hsa-mir-181b-5p	SLC7A11	23657
hsa-mir-181c-5p	SLC7A11	23657
hsa-mir-181d-5p	SLC7A11	23657
hsa-mir-183-3p	SLC7A11	23657
hsa-mir-191-5p	SLC7A11	23657
hsa-mir-196a-5p	SLC7A11	23657
hsa-mir-196b-5p	SLC7A11	23657
hsa-mir-197-5p	SLC7A11	23657
hsa-mir-199a-3p	SLC7A11	23657
hsa-mir-199b-3p	SLC7A11	23657
hsa-mir-20a-3p	SLC7A11	23657
hsa-mir-217	SLC7A11	23657
hsa-mir-221-3p	SLC7A11	23657
hsa-mir-222-5p	SLC7A11	23657

Table S3 (continued)

Table S3 (continued)

ID	Target	TargetID
hsa-mir-26a-5p	SLC7A11	23657
hsa-mir-27b-3p	SLC7A11	23657
hsa-mir-301a-3p	SLC7A11	23657
hsa-mir-301b-3p	SLC7A11	23657
hsa-mir-30b-5p	SLC7A11	23657
hsa-mir-30c-5p	SLC7A11	23657
hsa-mir-30d-5p	SLC7A11	23657
hsa-mir-30e-5p	SLC7A11	23657
hsa-mir-3140-3p	SLC7A11	23657
hsa-mir-330-3p	SLC7A11	23657
hsa-mir-331-5p	SLC7A11	23657
hsa-mir-33a-5p	SLC7A11	23657
hsa-mir-34c-3p	SLC7A11	23657
hsa-mir-361-5p	SLC7A11	23657
hsa-mir-362-5p	SLC7A11	23657
hsa-mir-374a-3p	SLC7A11	23657
hsa-mir-374b-5p	SLC7A11	23657
hsa-mir-378g	SLC7A11	23657
hsa-mir-411-3p	SLC7A11	23657
hsa-mir-4317	SLC7A11	23657
hsa-mir-4517	SLC7A11	23657
hsa-mir-4766-3p	SLC7A11	23657
hsa-mir-500a-5p	SLC7A11	23657
hsa-mir-5010-3p	SLC7A11	23657
hsa-mir-501-5p	SLC7A11	23657
hsa-mir-513a-5p	SLC7A11	23657
hsa-mir-542-3p	SLC7A11	23657
hsa-mir-548at-5p	SLC7A11	23657
hsa-mir-548b-3p	SLC7A11	23657
hsa-mir-561-3p	SLC7A11	23657
hsa-mir-580-3p	SLC7A11	23657
hsa-mir-622	SLC7A11	23657
hsa-mir-624-5p	SLC7A11	23657
hsa-mir-654-5p	SLC7A11	23657
hsa-mir-935	SLC7A11	23657
hsa-mir-99a-5p	SLC7A11	23657
hsa-mir-1-3p	SLC7A11	23657
hsa-mir-103a-3p	SLC7A11	23657
hsa-mir-124-3p	SLC7A11	23657

Table S3 (continued)

Table S3 (continued)

ID	Target	TargetID
hsa-mir-494-3p	SLC7A11	23657
hsa-mir-503-5p	SLC7A11	23657
hsa-let-7b-5p	SLC7A11	23657
hsa-mir-10b-5p	SLC7A11	23657
hsa-mir-126-3p	SLC7A11	23657
hsa-mir-129-2-3p	SLC7A11	23657
hsa-mir-146a-5p	SLC7A11	23657
hsa-mir-147a	SLC7A11	23657
hsa-mir-182-5p	SLC7A11	23657
hsa-mir-200c-3p	SLC7A11	23657
hsa-mir-203a-3p	SLC7A11	23657
hsa-mir-205-5p	SLC7A11	23657
hsa-mir-214-3p	SLC7A11	23657
hsa-mir-224-5p	SLC7A11	23657
hsa-mir-375	SLC7A11	23657
hsa-mir-376a-5p	SLC7A11	23657
hsa-mir-452-5p	SLC7A11	23657
hsa-mir-671-5p	SLC7A11	23657
hsa-mir-7-5p	SLC7A11	23657
hsa-mir-941	SLC7A11	23657
hsa-mir-101-3p	SLC7A11	23657
hsa-mir-374a-5p	SLC7A11	23657
hsa-mir-122	SLC7A11	23657
hsa-mir-103a-3p	NQO1	1728
hsa-mir-107	NQO1	1728
hsa-mir-186-5p	NQO1	1728
hsa-mir-24-3p	NQO1	1728
hsa-mir-338-5p	NQO1	1728
hsa-mir-34a-5p	NQO1	1728
hsa-mir-375	NQO1	1728
hsa-mir-485-5p	NQO1	1728
hsa-mir-1-3p	NQO1	1728
hsa-mir-124-3p	NQO1	1728
hsa-mir-126-3p	NQO1	1728
hsa-mir-128-3p	NQO1	1728
hsa-mir-129-2-3p	NQO1	1728
hsa-mir-147a	NQO1	1728
hsa-mir-200c-3p	NQO1	1728
hsa-mir-205-5p	NQO1	1728

Table S3 (continued)

Table S3 (continued)

ID	Target	TargetID
hsa-mir-210-3p	NQO1	1728
hsa-mir-27a-3p	NQO1	1728
hsa-mir-7-5p	NQO1	1728
hsa-mir-941	NQO1	1728
hsa-mir-374a-5p	NQO1	1728
hsa-mir-17-3p	GPX2	2877
hsa-mir-335-5p	GPX2	2877
hsa-mir-1343-3p	GPX2	2877
hsa-mir-23b-3p	GPX2	2877
hsa-mir-124-3p	GPX2	2877
hsa-mir-191-5p	GPX2	2877
hsa-mir-210-3p	GPX2	2877
hsa-mir-517a-3p	GPX2	2877
hsa-mir-98-5p	AKR1C3	8644
hsa-mir-155-5p	AKR1C3	8644
hsa-mir-16-2-3p	AKR1C3	8644
hsa-mir-1-3p	AKR1C3	8644
hsa-mir-1343-3p	AKR1C3	8644
hsa-mir-23b-3p	AKR1C3	8644
hsa-mir-10b-5p	AKR1C3	8644
hsa-mir-129-2-3p	AKR1C3	8644
hsa-mir-146a-5p	AKR1C3	8644
hsa-mir-15b-3p	AKR1C3	8644
hsa-mir-195-5p	AKR1C3	8644
hsa-mir-200b-3p	AKR1C3	8644
hsa-mir-203a-3p	AKR1C3	8644
hsa-mir-21-3p	AKR1C3	8644
hsa-mir-210-3p	AKR1C3	8644
hsa-mir-212-3p	AKR1C3	8644
hsa-mir-221-3p	AKR1C3	8644
hsa-mir-222-3p	AKR1C3	8644
hsa-mir-26a-5p	AKR1C3	8644
hsa-mir-27a-5p	AKR1C3	8644
hsa-mir-29a-3p	AKR1C3	8644
hsa-mir-29c-3p	AKR1C3	8644
hsa-mir-483-5p	AKR1C3	8644
hsa-mir-374a-5p	AKR1C3	8644
hsa-mir-1-3p	AKR1C1	1645
hsa-mir-155-5p	AKR1C1	1645

Table S3 (continued)**Table S3** (continued)

ID	Target	TargetID
hsa-mir-130a-3p	AKR1C1	1645
hsa-mir-195-5p	AKR1C1	1645
hsa-mir-27a-3p	AKR1C1	1645
hsa-mir-374a-5p	AKR1C1	1645